Residual Effect and N Fertilizer Rate Detection by High-Resolution VNIR-SWIR Hyperspectral Imagery and Solar-Induced Chlorophyll Fluorescence in Wheat

María D. Raya-Sereno, María Alonso-Ayuso, José L. Pancorbo, José L. Gabriel, Carlos Camino, Pablo J. Zarco-Tejada, and Miguel Quemada

***Abstract*—Adjusting nitrogen (N) fertilization and accounting for the legacy of past N fertilizer application (i.e., residual N) based on remote sensing estimation of crop nutritional status may increase resource efficiency and promote sustainable management of cropping systems. Our main goal was to evaluate the potential of hyperspectral airborne imagers and ground-level sensors for identifying N fertilizer rates and the residual N effect from the previous crop fertilization in a maize/wheat rotation. A two-season field trial that provided various combinations of N rates and residual N response was established in central Spain. Ground-level sensors and aerial hyperspectral images were used to calculate vegetation indices (VIs). In addition, the solar-induced chlorophyll fluorescence (SIF_{760}) was estimated by the Fraunhofer line-depth method using high-resolution hyperspectral imagery, and together with biophysical modeling, biochemical and biophysical constituents at canopy scales were retrieved. N uptake, N output, grain N concentration, and proximal sensors discriminated between different N fertilizer rates and identified the residual effect when it was relevant. Structural, photosynthetic pigments and short-wave infrared region (SWIR)-based VIs, together with SIF_{760} and the chlorophyll $a+b$ (C_{ab}), biomass, and the leaf area index (LAI), performed similarly on N rate detection. However, the residual effect of nitrification inhibitors was only detected by the structural (NDVI and OSAVI), chlorophyll (CCCI and NDRE), blue/green, NIR-SWIR ($N_{850,1510}$) indices, SIF_{760}, C_{ab}, biomass, and the LAI. This study confirmed the ability of remote sensing to identify N rates at early growth stages and highlighted its potential to detect residual N in crop rotation.**

***Index Terms*—Nitrification inhibitors, precision farming, proximal sensors, radiative transfer model, remote sensing, soil N pool, vegetation indices (VIs).**

I. Introduction

The use of nitrogen (N) mineral fertilizers has increased in the last few decades, and its demand will reach 119 million tons by the end of 2021 [1]. However, only about half of the N applied is assimilated by crops [2], whereas a large fraction is released to the environment, contributing to groundwater pollution, ammonia redeposition, global warming, and stratospheric ozone depletion [3]. Improving fertilizer management through the optimization of the timing and fertilizer rate is essential for reducing the environmental impact while maintaining crop productivity [4]. Proximal and remote sensors are rapid, nondestructive, and highly accurate tools that can contribute to optimizing N fertilizer use since they provide measurements or indices that are sensitive to crop N status [5]. Recent research has emphasized that the N supply to crops not only comes from the fertilizer applied each year but also from the previous fertilization legacy, which is called residual N [6], [7]. The importance of the residual N effect arises when fertilizer application approaches suboptimal levels, and so it is particularly relevant in countries seeking a reduction in N fertilizer use due to environmental concerns [8]. A lot of research has been devoted to using sensors to identify crop differences between various levels of fertilizer application [9], [10]; however, detecting the residual N effect with proximal or remote sensors remains a challenge.

Determining the residual N supplied by the soil is complicated to implement at the field scale because the sources are multiple and the analysis uncertain. Measuring soil mineral

Manuscript received March 11, 2021; revised June 6, 2021 and July 16, 2021; accepted July 19, 2021. This work was supported in part by the Spanish Ministry of Education under Grant FPU17/01251, in part by the Ministry of Economy and Competitiveness under Grant AGL2017-83283-C2-1-R and Grant PRE2018-084215, in part by the Comunidad de Madrid, Spain, under Grant AGRISOST-CM S2018/BAA-4330, and in part by EuroChem Agro. *(Corresponding author: Miguel Quemada.)*

María D. Raya-Sereno, José L. Pancorbo, and Miguel Quemada are with the Department of Agricultural Production, Universidad Politécnica de Madrid, 28040 Madrid, Spain, and also with the Research Centre for the Management of Agricultural and Environmental Risks (CEIGRAM), Universidad Politécnica de Madrid, 28040 Madrid, Spain (e-mail: md.raya@upm.es; joseluis.pancorbo@upm.es; miguel.quemada@upm.es).

María Alonso-Ayuso is with the Soil Management and Global Change Group, Spanish National Research Council (CSIC), 50059 Zaragoza, Spain (e-mail: malonso@eead.csic.es).

José L. Gabriel is with the Instituto Nacional de Investigación y Tecnología Agraria y Alimentaria (INIA), 28040 Madrid, Spain, and also with the Research Centre for the Management of Agricultural and Environmental Risks (CEIGRAM), Universidad Politécnica de Madrid, 28040 Madrid, Spain (e-mail: gabriel.jose@inia.es).

Carlos Camino is with the European Commission (EC), Joint Research Centre (JRC), 21027 Ispra, Italy (e-mail: caminoccg@gmail.com).

Pablo J. Zarco-Tejada is with the Faculty of Veterinary and Agricultural Sciences (FVAS), School of Agriculture and Food, The University of Melbourne, Melbourne, VIC 3010, Australia, also with the Department of Infrastructure Engineering, Faculty of Engineering and Information Technology (FEIT), The University of Melbourne, Melbourne, VIC 3010, Australia, and also with the Instituto de Agricultura Sostenible (IAS), Consejo Superior de Investigaciones Científicas (CSIC), 14004 Córdoba, Spain (e-mail: pablo.zarco@unimelb.edu.au).

This article has supplementary downloadable material available at https://doi.org/10.1109/TGRS.2021.3099624, provided by the authors.

Digital Object Identifier 10.1109/TGRS.2021.3099624

available N is used to adjust N fertilization but is not enough to account for the residual effect, as other N sources, such as the soil organic matter pool, microbial biomass, or crop residues and roots, are not accounted for [11]. Available N is slowly released from these sources during the crop growth, and estimating the crop nutritional status might allow identifying the residual effect and adjusting N fertilizer application to crop requirements. In long-term field experiments in France, Sebilo *et al.* [6] estimated that 12%–15% of the fertilizer applied was still present in the soil N pools 30 years after application and continued to be released, either to be taken up by crops or to leak toward groundwaters. In China, the residual N fertilizer taken up by crops in the years after application obtained from comparison of long- and short-term experiments was estimated at 10%–18% of the applied fertilizer N [12]. Lower amounts (6.5%) of residual N recovered by crops during the subsequent five seasons were reported in a summary of experiments conducted in Africa, South America, and Asia [13]. Therefore, the residual N effect is usually a minor source of N compared to the annual application; however, the cumulative effect should be considered when developing strategies to increase fertilizer N efficiency.

The use of nitrification inhibitors is a reliable technique to mitigate N gaseous emissions to the atmosphere and, in some cases, to improve fertilizer use efficiency [14]. N fertilizers blended with nitrification inhibitors delay the oxidation of ammonium to nitrate, mitigating N losses but also enhancing soil N retention [15]. Studies focused on the enhancement of the residual N effect in the subsequent crop caused by the application of nitrification inhibitors are limited [16]–[18] and show that the relevance depends on soil and local conditions [19]. Detection of the residual effect after nitrification inhibitors could allow a better adjustment of fertilizer application to the subsequent crop and contribute to sustainable management of N fertilization in crop rotations.

Remote sensing estimation of the crop N nutritional status is a valuable tool to support fertilization management and is based on the spectral properties of plants [20]. Most of the vegetation indices (VIs) that estimate crop status use narrow bands placed in the visible and near-infrared region (VNIR) [21]. Other VIs use solely the short-wave infrared region (SWIR) to assess the N content directly [22]. In this regard, recent studies have found a better estimation of plant N concentration using VIs that included wavelengths in the SWIR using a hand-held FieldSpec spectroradiometer [23] or aerial sensors [24], [25]. Nevertheless, the VIs do not employ all the relevant spectral information, and consequently, several studies demonstrated that the radiative transfer models enhanced transferability and robustness compared to the VIs [26]–[28]. However, few studies have highlighted the utility of physical models for the accurate estimation of leaf N content [25], [29]. In this regard, Wang *et al.* [29] showed that the model estimated leaf parameters (leaf chlorophyll content, leaf mass per area, and equivalent water thickness) were able to successfully track the N content.

Moreover, physical models have the advantage of providing explicit representation of the interactions between electromagnetic radiation and vegetation structures, allowing direct simulation and inversion of the reflectance acquired [30]. In this context, the leaf optical properties (PROSPECT) and the scattering by arbitrary inclined leaves (SAIL) models are usually coupled (PROSAIL) to simulate bidirectional reflectance and estimate biochemical and biophysical parameters simultaneously [26]. Applying PROSAIL to wheat, several authors found that inverted chlorophyll [31] and the leaf area index (LAI) [27] were reliable indicators of plant traits to estimate wheat N status. These models are constantly evolving, and a new PROSPECT version (PROSPECT-PRO) developed by Féret *et al.* [30] directly estimated N content in leaf proteins, opening the opportunity to improve N rates and residual effect detection.

On another note, the use of chlorophyll fluorescence is another approach to diagnose vegetation status, based on the electromagnetic signal emitted in the 650–850-nm spectrum wavelengths as a response to photosynthesis [32]. Chlorophyll fluorescence is a direct proxy for electron transport rate and, hence, photosynthetic activity [33]. It is well documented that N deficiency could affect photosystem II photochemistry, lowering the photochemical efficiency, quantum yield electron transport, and, therefore, the assimilation rate [34], [35]. In addition, SIF_{760} is strongly correlated to the leaf-level maximum carboxylation rate (Vcmax) of the enzyme Rubisco [36], which is probably one of the most abundant proteins on earth and a major sink for plant N. Thus, the use of SIF_{760} can help to improve the estimation of N status due to the direct link between fluorescence emission and plant photosynthesis.

In addition, chlorophyll fluorescence can be measured with active methods based on pulse-amplitude modulation fluorometer systems [37] or laser-induced fluorescence [38]. However, at the field scale, the use of active techniques that rely on artificial light to excite the leaf is limited. Instead, passive methods that the SIF_{760} is based on solar irradiance and the radiance emitted by vegetation through the use of atmospheric O_2 absorption features [39] allow application at a regional scale. Therefore, passive methods are a tool widely used for detecting plant diseases [40]–[42] and water stress in woody and cereal crops [43]. However, to date, few studies have used SIF_{760} to assess the crop N status [44]. In this regard, some studies have demonstrated the link between chlorophyll fluorescence and photosynthetic activity at leaf and canopy levels [45], [46]; Camino *et al.* [25] found that the physical models that included SIF_{760} achieved higher accuracy in predicting N concentration in wheat than models built only with inverted chlorophyll $a+b$ (C_{ab}), dry matter (C_m), or equivalent water thickness (C_w), suggesting that SIF_{760} could contribute to the detection of crop N status and residual effect. Therefore, we further explored, in this study, the capability of fluorescence emission retrievals for the detection of crop N status and residual effect.

Finally, agronomic studies confirmed that the best indicator to determine crop N status is the N nutrition index (NNI), which estimates the N required for maximum growth as the ratio between the actual crop N concentration and the critical N concentration [47]. The critical N concentration is the minimum N concentration (%N) needed for providing the maximum growth rate for given biomass. In many field studies, the NNI has been successfully applied to various

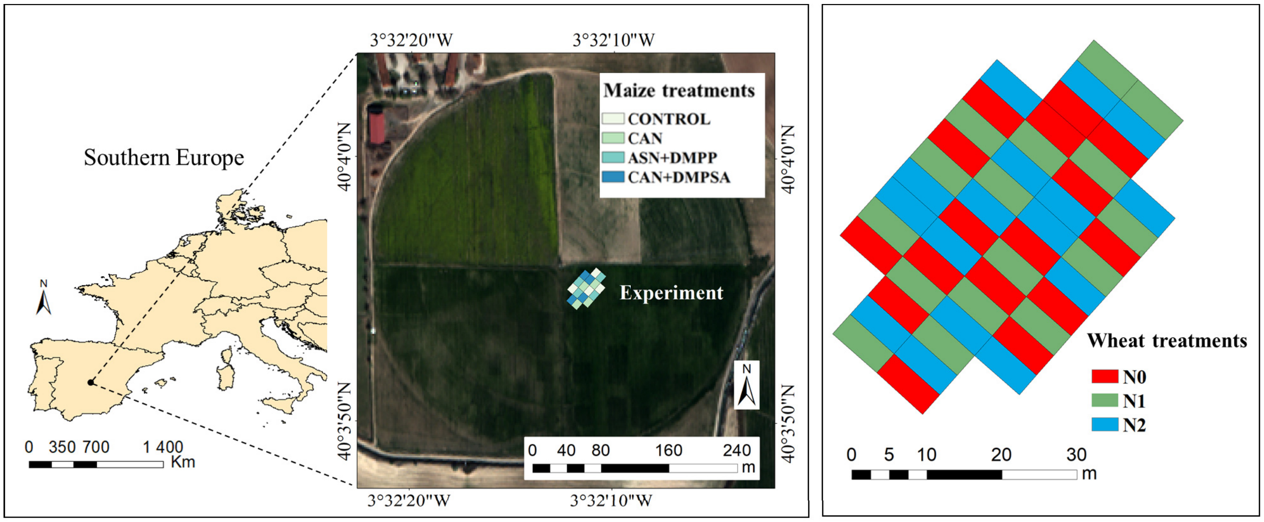

(a) (b)

Fig. 1. Study area of the field experiment in Aranjuez, Madrid, Central Spain, Southern Europe. (a) Location of the experiment with the different maize N treatments established in 2018. (b) Split-plot of wheat experiment in three different N rates in 2019.

crops, including wheat [48]–[50]. Therefore, the ability of a sensor, proximal or remote, to assess NNI is a reference for its potential to support N management.

For these reasons, the general objective of this study was to evaluate the capacity of ground-level and hyperspectral aerial sensors to improve N assessment in winter wheat (*Triticum aestivum* L.). Specific research addressed: 1) the capacity of innovative spectral plant traits quantified by each of the sensors to distinguish among N fertilization rates and 2) the potential of identifying the residual N effect from previous years' fertilization. To this purpose, the performance of ground-level sensors, by plant traits estimated by physical model inversion, as well as SIF_{760} and VIs based on VNIR and SWIR to assess grain yield, grain N concentration, N exported in grain (N output), and the NNI, was evaluated.

II. Material and Methods

A. Field Experiment

The field experiment was established at the Chimenea research station (40°03′ N, 03°31′ O, and 550 m a.s.l.) located in Aranjuez (Madrid, Spain). The climate is classified according to Köppen as a cold semiarid climate (Bsk), with a hot, dry summer. The mean annual temperature is 14.2 °C, and the cumulated annual rainfall is 373 mm, which mainly takes place in autumn and spring. Weather data were recorded by a climatic station located 100 m from the field plot. The soil at the field site is classified as *Haplic calcisol* [51]; it has medium topsoil organic matter content (10.1 g kg^{-1} organic carbon and 1.0 g kg^{-1} total N) and a silty clay loam texture with low stone content and pH $\approx$ 8.1 throughout the soil profile. More details on the soil characteristics can be found in [52].

A maize/wheat rotation was conducted from April 2018 to July 2019, and the experiment was designed to study crop N status under different fertilizer rates and to identify the residual effect of mineral fertilizers on bread wheat (*Triticum aestivum* L., cv. Nogal). The experiment was sown with maize (*Zea mays* L., Pioneer P1574, FAO 700) in April 2018 at a plant density of 80 000 seeds ha^{-1}. Sixteen plots (8 m × 10.5 m) were randomly distributed in four treatments with four replications [see Fig. 1(a)]. The treatments were: Control (no N application), conventional fertilizer calcium ammonium nitrate (CAN, 27% N) and ammonium sulfate nitrate (ASN, 26% N) blended with the nitrification inhibitor 3, 4-dimethylpyrazole phosphate (DMPP) (ASN + DMPP); CAN enriched with sulfur (CAN(S), 27% N) together with the nitrification inhibitor 3, 4-dimethylpyrazole succinic (DMPSA) (CAN+DMPSA). All fertilizer treatments received the recommended rate (200 kg N ha^{-1}). After the maize harvest (October 2018), wheat (*Triticum aestivum* L., cv. Nogal) was planted on November 15, 2018, at a rate of 220 kg ha^{-1}, and each plot was split into three subplots (3.5 m × 8 m) [see Fig. 1(b)]. Each subplot received no N (N0), conventional fertilizer (CAN, 27% N) to provide N available at the recommended rate (150 kg N ha^{-1}; N1), or an extra N rate for increasing grain N content (190 kg N ha^{-1}; N2) (see Fig. 1(b) and Table I).

N fertilizer was split into two applications and hand-broadcasted to plots in two growth stages (GSs) [53]: over the maize crop at three leaves unfolded (GS13, 28/05/2018) and stem elongation (GS38, 02/07/2018); and over the wheat crop at tillering (GS22, 30/01/2019) and at the end of stem elongation (GS39, 15/04/2019) (see Table I). The N available for wheat was obtained by adjusting the fertilizer rates according to the inorganic N content in the upper 0.50-m soil layers, determined before the first N application (January 30). Before sowing the crops, 70 kg ha^{-1} P_2O_5 and 120 kg ha^{-1} K_2O were applied to all plots to ensure phosphorus and potassium availability. After harvest, the residues of both crops were incorporated into the soil.

TABLE I
WHEAT N FERTILIZER APPLIED IN THE EXPERIMENT AND TOTAL N AVAILABLE FOR THE VARIOUS N RATE TREATMENTS IN 2019, DEPENDING ON 2018 TREATMENTS

Treatments		First fertilizer application (GS22)	Second fertilizer application (GS39)	Total N available*
2018	**2019**	**kg N ha^{-1}**	**kg N ha^{-1}**	**kg N ha^{-1}**
Control	N0	0	0	60
	N1	50	40	150
	N2	50	80	190
Fertilized	N0	0	0	118
	N1	50	0	168
	N2	50	40	208

*Applied fertilizer plus inorganic N content in the upper 0.5 m of the soil profile just before fertilizer application. The inorganic N content was 60 kg N ha^{-1} in Control treatment and 118 kg N ha^{-1} in fertilized treatments.

During spring and summer, irrigation water was delivered using a center-pivot system to match crop evapotranspiration calculated using daily local data. The total water input was 732 mm for maize in the first season and 209 mm for wheat in the second season. Wheat suffered water stress during winter due to scarce rainfall and limited irrigation water availability.

B. Crop Analysis

In the first season, a central 1.5-m-wide strip was harvested from each plot using an experimental combiner, leaving a 1-m buffer at the beginning and end of each plot. A grain subsample was oven-dried (65 °C) and weighed to correct maize yield by moisture content.

In the second season, a sample of wheat plants from a 0.25-m^2 square was hand-harvested at flowering (GS65) in all plots of the experiment when maximum N uptake was expected. A subsample of each plant component (spikes and the rest of the aboveground biomass) was oven-dried (65 °C), weighed, and ground. At harvest, a central 1.4-m-wide strip was harvested from each plot by an experimental combiner, leaving a 1-m buffer at the beginning and end of each plot. A grain subsample from each plot was oven-dried (65 °C), weighed, ground, and saved for analysis. The total N concentration of plant components was determined by the Dumas combustion method (LECO FP-428 analyzer, St. Joseph, MI, USA). The N content of plant components was calculated by multiplying dry biomass (kg ha^{-1}) by N concentration (%N). At flowering, the wheat crop N uptake (kg N ha^{-1}) was calculated by totaling the N content in spikes and the rest of the aboveground biomass, and the NNI was calculated as the ratio between the actual crop N concentration and the critical N concentration that allows maximum growth for given biomass [48]. The critical N concentration was obtained from Pancorbo *et al.* [50] who developed an N dilution curve for a winter wheat crop under similar environmental conditions. At harvest, N output (kg N ha^{-1}) was calculated as the product of grain yield (kg ha^{-1}) multiplied by grain N concentration (%N).

C. Soil Inorganic N Content (N_{min})

In the experiment, soil samples were taken to determine the soil inorganic N (N_{min}) before the first topdressing of N fertilizer in wheat (January 2019). Three soil cores per plot were taken and combined by soil layer. Samples were taken by 0.25-m intervals down to a 0.50-m depth with an Eijkelkamp helicoidal auger (Eijkelkamp Agrisearch Equipment, Geisbeek, The Netherlands). Samples were placed in a plastic box and firmly closed immediately, transported, and refrigerated (4 °C–6 °C). Within the five subsequent days, a soil subsample from each box was extracted with 1 M KCl (~30 g of soil: 150 ml of KCl), centrifuged, and decanted, and a subsample of the supernatant volume was stored in a freezer until later analysis. The nitrate concentration was determined by the Griess–Ilosvay method [54] and ammonium by the salicylate-hypochlorite method [55]. Nitrate (NO_3^--N) and ammonium (NH_4^+-N) contents were calculated for each layer and plot, and N_{min} as the sum of nitrate and ammonium content.

D. Ground-Level Optical Measurements

Different commercial optical sensors were used to assess N fertilization rates and the residual effect on the wheat, coming from the different fertilizer treatments applied in the previous season. The two devices chosen were Dualex Scientific (Force-A, Orsay, France) and GreenSeeker (Handheld Crop Sensor Model HCS-100, Trimble, Sunnyvale, CA, USA).

The Dualex Scientific is a leaf clip sensor that estimates the crop N status and measures chlorophyll (Chl) content as the difference between the light transmitted at the far red (710 nm) and the infrared wavelengths (850 nm) [56]. In addition, this device measures leaf epidermal flavonoid (Flav) and anthocyanin (Anth) content, based on the screening effect of polyphenols on chlorophyll fluorescence [56]. Chlorophyll fluorescence is induced by a reference red LED that is transmitted through the epidermis without being absorbed by polyphenols and by a second specific light (UV for Flav and green for Anth) absorbed by polyphenols. The ratio of chlorophyll fluorescence emitted under red and UV excitation provides the Flav and under read and green provides the Anth content per unit of leaf area. The N balance index (NBI) is calculated as the ratio between the Chl and Flav contents.

The GreenSeeker is an active light proximal sensor that generates its own red and near-infrared (NIR) lights for measuring the normalized difference vegetation index (NDVI). Measurements are taken 1 m above the crop surface, and the GreenSeeker readings are calculated as $(R_{\mathrm{NIR}}\text{-}R_{\mathrm{Red}})/(R_{\mathrm{NIR}} + R_{\mathrm{Red}})$, where R_{NIR} is the reflectance of active NIR light (774 nm) and R_{Red} is the reflectance of the active red light (656 nm).

Readings with both optical sensors were taken at ground level at three different GSs: initial stem elongation (GS32), end of stem elongation (GS39), and full flowering (GS65). On each sampling date, six measurements were taken per plot, and the representative value was determined as the average of the readings. Dualex measurements were taken at the uppermost fully developed leaf, avoiding midribs.

E. Remote Sensing Data Collection

Ground-level measurements were synchronized with airborne hyperspectral image acquisition carried out at the same three sampling dates (GS32: 11/03/2019; GS39: 12/04/2019; and GS65: 16/05/2019). All subplots were georeferenced with real-time kinematic technology to compare different VIs and wheat inverted parameters with ground-level measurements. A perimeter buffer (1 m) was considered for extracting spectral information from each plot to ensure that readings were representative of each treatment.

1) Aircraft Hyperspectral Imagery: The hyperspectral images were taken under clear sky conditions onboard a Cessna aircraft flying at 330 m over the experimental plots and 70 knots ground speed with heading on the solar plane at 11 GMT using a VNIR hyperspectral imager (Hyperspec VNIR model, Headwall Photonics, Fitchburg, MA, USA) and a Hyperspec linear array imager (NIR-100 model, Headwall Photonics, Fitchburg, MA, USA). The VNIR hyperspec sensor captured reflectance in the 400–850-nm spectral region with a spectral resolution of 6.5-nm full-width at half-maximum (FWHM) and a spatial resolution of 0.2 m, and the hyperspec NIR-100 sensor covered the 950–1750-nm region with 165 spectral bands at the 16-bit radiometric resolution, with 6.05-nm FWHM with a spatial resolution of 0.6 m. Hyperspec VNIR and NIR-100 sensors were radiometrically calibrated with an integrating sphere (CSTM-USS-2000C LabSphere, North Sutton, NH, USA) using four levels of illumination and six integration times. Atmospheric correction of the hyperspectral images was performed using incoming irradiance measured with a field spectrometer and simulated by the SMARTS model [57], [58]. In addition, we conducted an empirical line calibration [59] using field-measured spectra to ensure the radiometric quality of the hyperspectral imagery and remove spectral noise. For that, we acquired reflectance measurements at the flight time over soil surfaces using a handheld field spectrometer (Analytical Spectral Devices, Boulder, CO, USA). Orthorectification of hyperspectral imagery was performed following Zarco-Tejada *et al.* [46]. Spectral data were smoothed using the Savitzky–Golay method with a filter length of 9 interpolated to 1 nm. Wavelengths between 1085–1185 and 1320–1500 nm were removed due to atmospheric water vapor absorption.

2) Modeling Methods: We retrieved the canopy structural parameters (LAI and leaf angle distribution, LIDFa) and leaf biophysical and biochemical constituents from each plot using the PROSAIL-PRO model. The PROSAIL-PRO radiative transfer model couples the PROSPECT-PRO leaf reflectance model [30] and the 4SAIL turbid medium canopy radiative transfer model [60]. PROSPECT-PRO enabled the separation of the N-based constituents (proteins) from the carbon-based constituent (including cellulose, lignin, hemicellulose, starch, and sugars). The SAIL model is based on the 1-D model developed by Suits [61] to simulate the bidirectional reflectance of a canopy. The inversion of PROSAIL-PRO consisted of an iterative-optimization numerical approach to estimate leaf traits and canopy parameters from reflectance across the observed hyperspectral spectrum. The inversion method estimated the root mean square error (RMSE) between the simulated reflectance and the hyperspectral image reflectance by successive input parameter iteration. The iterative optimization process selected the simulated spectra with the lowest RMSE with respect to the observed spectra. Then, we calculated the average for each plant trait based on the selected simulations (0.1–0.25%) with the lowest RMSE values [62]. The iterative-optimization numerical approach was designed to estimate the average of the best modeled spectra that yielded the best fit against the observed spectra.

To invert each leaf and canopy traits using the coupled PROSAIL-PRO model, we built a lookup table (LUT) of 20 000 simulations for the proposed inversion method. The input variables and their ranges in the PROSPECT-PRO and 4SAIL models are shown in Table S1 in the Supplementary Material. The input parameters were constrained to specific ranges to avoid potential ill-posed inversion solutions. In particular, we used uniform distribution for the main parameters, except for C_w and C_m for which a Gaussian distribution was used. The ranges were established based on field measurements (i.e., Dualex readings) and existing literature. The resulting LUT covered the variability of wheat canopies measured by both hyperspectral sensors. The solar geometry and the viewing angles needed to simulate canopy reflectance were extracted for the flight date. All reflectance spectra simulated were convoluted to the bandwidth of the hyperspectral sensors used in this study. The spectral convolution was conducted through a Gaussian band spectral response function using the FWHM of each sensor (6.5 nm for the VNIR hyperspectral sensor and 6.05 nm for the NIR-100 hyperspectral sensor).

In this study, the spectral range between 400 and 800 nm measured with the hyperspec VNIR camera was used to estimate C_{ab}, carotenoids (Car), and anthocyanin (Anth), while the 400–1700-nm spectral region was used to retrieve structural parameters (LAI and LIDFa), C_w and C_m. In addition, the biomass (i.e., LAI $\times$ C_m g/cm^2) was also calculated to compare its estimation with biomass field measurement.

The accuracy of the parameters estimated with model inversion was evaluated by the RMSE calculated between the

TABLE II
VEGETATION INDEX EQUATIONS USED IN THIS STUDY FOR HYPERSPECTRAL DATA

Indices	Equation	Reference
	Greenness or structural indices	
Normalized difference vegetation index	$NDVI = (R_{800} - R_{670})/(R_{800} + R_{670})$	[64]
Optimized soil-adjusted vegetation index	$OSAVI = (1 + 0.16) \times (R_{800} - R_{670})/(R_{800} + R_{670} + 0.16)$	[65]
	Photosynthetic pigment indices	
	Xanthophyll indices	
Photochemical reflectance index (570)	$PRI = (R_{570} - R_{531})/((R_{570} + R_{531})$	[66]
Photochemical reflectance index (670 and 570)	$PRIm4 = (R_{570} - R_{531} - R_{670})/((R_{570} + R_{531} + R_{670})$	[67]
	Blue/green/red ratio	
Blue/green index	$BGI1 = R_{400}/R_{550}$	[28]
Blue/red index	$BRI1 = R_{400}/R_{690}$	[43]
	Chlorophyll-related indices	
Transformed chlorophyll absorption in reflectance index	$TCARI = 3\ [(R_{700} - R_{670}) - 0.2^* (R_{700} - R_{550})^*(R_{700}/R_{670})]$	[68]
Modified chlorophyll absorption in reflectance index	$MCARI = [(R_{700} - R_{670}) - 0.2\ (R_{700} - R_{550})](R_{700}/R_{670})$	[21]
Combined TCARI/OSAVI	TCARI/OSAVI	[68]
Double peak canopy nitrogen index	$DCNI = (R_{720} - R_{700})/(R_{700} - R_{670})/(R_{720} - R_{670} + 0.03)$	[69]
Normalized difference red edge	$NDRE = (R_{790} - R_{720})/(R_{790} + R_{720})$	[70]
Canopy chlorophyll content index	$CCCI = (NDRE - NDRE_{min})/(NDRE_{max} - NDRE_{min})$	[71]
Solar induced fluorescence (SIF_{760})	FLD method using 2 reference bands (750; 762)	[39]
	SWIR- and VNIR-SWIR-based indices	
Normalized difference nitrogen index	$NDNI = [\log(1/R_{1510}) - \log (1/R_{1680})]/[\log (1/R_{1510}) + \log (1/R_{1680})]$	[24]
$TCARI_{1510}$	$TCARI_{1510} = 3\ [(R_{700} - R_{1510}) - 0.2^* (R_{700} - R_{550})^*(R_{700}/R_{1510})]$	[23]
$MCARI_{1510}$	$MCARI_{1510} = [(R_{700} - R_{1510}) - 0.2\ (R_{700} - R_{550})](R_{700}/R_{1510})$	[23]
$TCARI/OSAVI_{1510}$	$TCARI_{1510}/OSAVI_{1510} = TCARI_{1510}/[(1+0.16) (R_{800}-R_{1510})/(R_{800}+R_{1510}+0.16)]$	[23]
$N_{1510, 660}$	$N_{1510,660} = (R_{1510} - R_{660})/(R_{1510} + R_{660})$	[23]
$N_{850,1510}$	$N_{850,1510} = (R_{850} - R_{1510})/(R_{850} + R_{1510})$	[25]

simulated and measured canopy spectral reflectances. Finally, the coefficient of determination (R^2) and RMSE between the retrieved biophysical parameters (C_{ab}, Car, Anth, biomass, and LAI) obtained by PROSAIL-PRO model inversion and the crop nutritional status was calculated to investigate their relationship.

3) Vegetation Indices and SIF_{760} Calculation: The average radiance and reflectance spectra calculated for each experimental plot were used to extract several VIs related to: 1) crop structure; 2) photosynthetic pigments (xanthophyll, blue/green/red, and chlorophyll); and 3) N content (see Table II). The VIs were related to greenness or crop structure when based on the normalized ratio between bands from the NIR and the visible or SWIR, to photosynthetic pigment when narrow bands from the red edge region were incorporated, and SWIR bands combined with NIR were used to build VIs related to N.

The solar-induced fluorescence (SIF_{760}) was estimated using the Fraunhofer line-depth (FLD) principle [39] by combining solar irradiance and radiance emitted by the canopy crop using the atmospheric O_2 absorption features [32]. This step is important when attempting to estimate SIF_{760} with coarser spectral resolution sensors (5–6 nm), mainly because the fluorescence emitted is strongly affected by scattering and reabsorption processes at the canopy level. Damm *et al.* [63] demonstrated that hyperspectral sensors with 5–6 nm FWHM spectral bands can be successfully used to estimate chlorophyll fluorescence using the FLD approach, which is traditionally estimated using instruments with a spectral resolution below 0.5 nm. The SIF_{760} signal calculated in this study was based

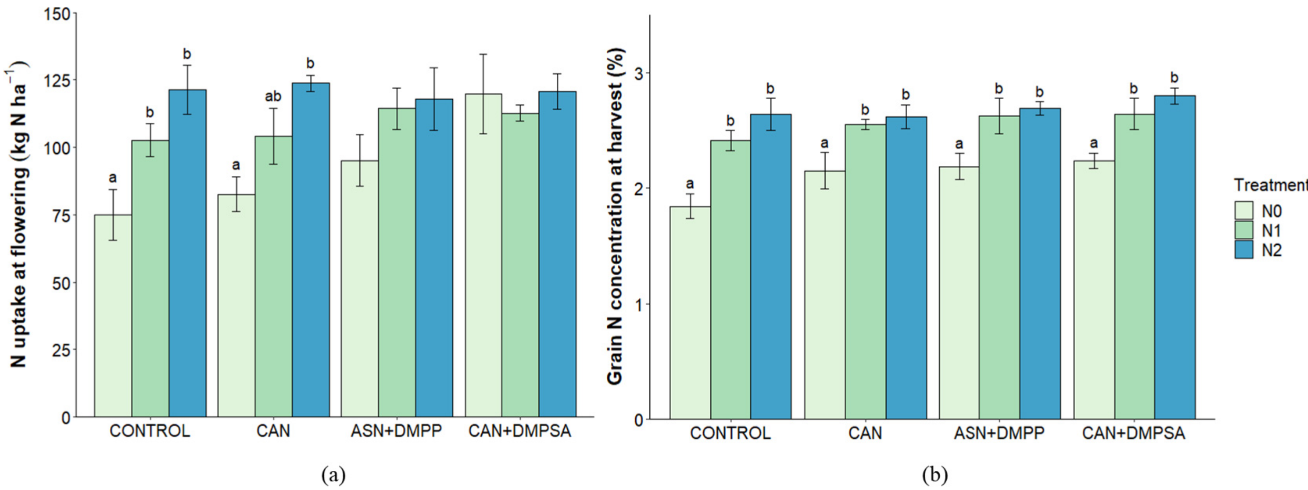

Fig. 2. (a) Wheat crop N uptake at flowering and (b) grain N concentration at harvest for the various N rate treatments (N0, N1, and N2) in 2019. Treatments on the X-axis were applied in the previous 2018 season. For further treatment descriptions, see the main text. Letters above bars indicate significant differences between wheat N rate treatments within the previous year's fertilizer treatments according to Tukey's test at $P \leq 0.05$.

on two spectral bands *in* and *out* of the O_2-A feature. The FLD method used the radiance L_{in} (L762 nm) and L_{out} (L750 nm) from the airborne imagery and the irradiance E_{in} (E762 nm) and E_{out} (E750 nm) from irradiance spectra concurrently measured at the time of the flights. We simulated the incoming irradiance using the SMARTS model [57], [58] according to the aerosol properties and weather conditions of the flights. For that, we used the aerosol properties (i.e., aerosol optical depth, Ångström exponent, and air mass) extracted from the nearest ground-based available observations from the AErosol RObotic NETwork (AERONET, http://aeronet.gsfc.nasa.gov). As a further step, the simulated irradiance was interpolated and convoluted to the bandwidth of the hyperspectral sensor.

F. Statistical Analysis

Statistical analyses were carried out to assess the potential of different sensors and parameters for detecting N rates and residual effect. After verification of data normality and variance homogeneity, a linear mixed model was used in crop data and sensor readings to evaluate their detection at three different GSs. The fertilizers applied in 2018, the N rates applied in 2019, and the interaction between them were considered as a fixed effect, whereas the subplot was considered as a random effect for the analysis of variance. In addition, one-way ANOVA was performed to determine differences between treatments of soil inorganic N content. Means were separated by Tukey's test at the 0.05 probability level ($P \leq 0.05$). Finally, the coefficient of determination (R^2) and RMSE were calculated to analyze the goodness of fit between the NNI and the sensor indicators of crop N status. All statistical analyses were performed using the software *R* [72].

III. Results

A. Crop Analysis

In the first season, the maize grain yield (14% moisture content) in Control (10.6 Mg ha^{-1}) was significantly lower than in the fertilized treatments, which did not present differences among them. In the second season, the average wheat grain yield was 3.9 Mg ha^{-1}, and no differences were found among treatments, probably due to the low winter rainfall that limited wheat tillering and yield (see Table S2 in the Supplementary Material). The response to second-year N fertilization became evident in the data collected at flowering (GS65) since the N uptake and NNI responded to fertilizer application when the previous year's treatments were Control or CAN (see Fig. 2(a), and see Table S2 in the Supplementary Material). At harvest, grain N reinforced the effect of the N fertilizer rates, as all treatments fertilized in 2019 increased grain N concentration [see Fig. 2(b)] and most grain N output (see Table S2 in the Supplementary Material) with respect to N0.

The N residual effect was observed at wheat flowering and harvest (see Fig. 3). At flowering, when comparing N uptake and NNI in the unfertilized wheat plots (N0), the treatment that received CAN + DMPSA in the previous year showed a higher value than Control (see Fig. 3(a), and see Table S2 in the Supplementary Material). In addition, the treatments that received fertilizer with nitrification inhibitors in 2018 (ASN + DMPP or CAN + DMPSA) did not show differences in N uptake and the NNI at flowering between N rates in 2019 (see Fig. 2(a), and see Table S2 in the Supplementary Material). At harvest, the N output in N0 wheat plots was higher following maize fertilized with CAN+DMPSA compared to the Control, while ASN+DMPP and CAN had intermediate values [see Fig. 3(b)].

Before wheat fertilization, there were no differences in N_{min} in the upper 0.5 m among maize fertilized treatments in 2018 (see Fig. S3 in the Supplementary Material). The previous fertilized treatments presented higher N_{min} (118 kg N ha^{-1}) than Control (60 kg N ha^{-1}), and the contribution of ammonium accounted for <10% of the total soil N_{min}.

B. Comparison Between Field-Measurements and Inverted Parameters

Considering the three GSs of this study, the best correlation between inverted and measured parameters was achieved by

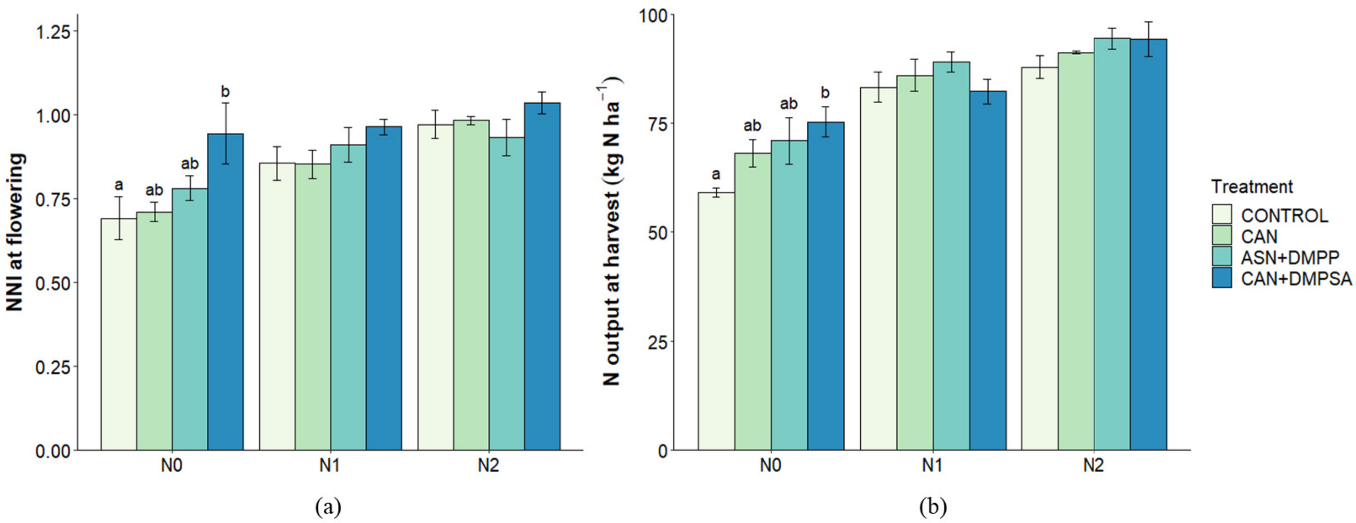

Fig. 3. (a) Wheat NNI at flowering and (b) N output at harvest for the various N rate treatments (N0, N1, and N2) applied in 2019. Treatments in the legend were applied in the previous 2018 season: 0 kg N ha^{-1} (Control) or 200 kg N ha^{-1} as CAN, as ASN blended with nitrification inhibitor 3, 4-dimethylpyrazole phosphate (ASN + DMPP) or as CAN blended with the nitrification inhibitor 3, 4-dimethylpyrazole succinic (CAN + DMPSA). Letters above bars indicate significant differences between maize fertilizer treatments the previous year within N rate treatments according to Tukey's test at $P \leq 0.05$.

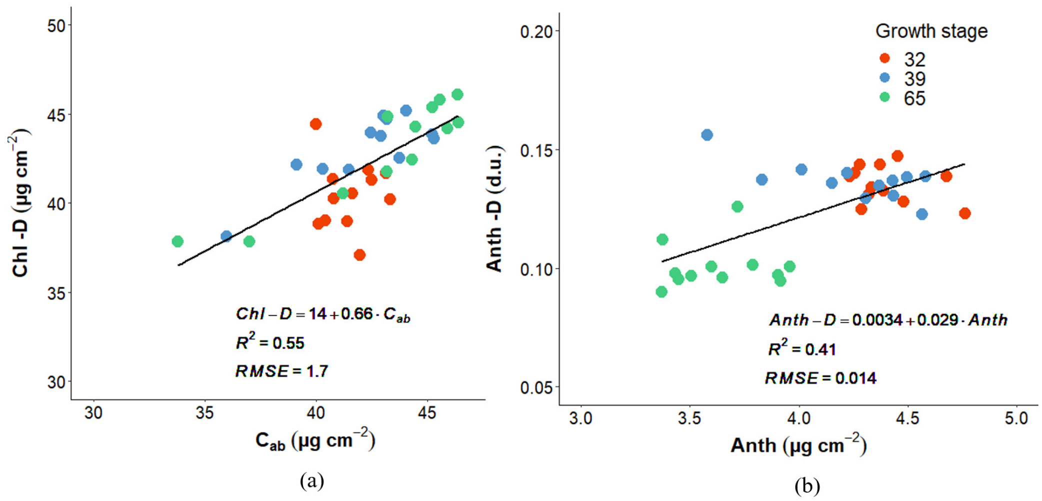

Fig. 4. Wheat pair values of (a) chlorophyll content (μg cm^{-2}) estimated by model inversion (C_{ab}) and measured with Dualex (Chl-D) and (b) anthocyanin (μg cm^{-2}) estimated by model inversion (Anth) and measured with Dualex (Anth-D, d.u: dualex units) at three GSs (symbols): initial stem elongation (GS32), end of stem elongation (GS39), and flowering (GS65). Each symbol is the mean value of each plot assigned to the various N rate treatments (N0, N1, and N2) applied in 2019. The solid line is the linear regression with the corresponding equation, the coefficient of determination (R^2), and RMSE.

chlorophyll concentration [$R^2 = 0.55$; see Fig. 4(a)], followed by anthocyanins [$R^2 = 0.41$; see Fig. 4(b)]. The chlorophyll relationship improved when only the values obtained at the end of stem elongation and flowering were considered [$R^2 = 0.78$; see Fig. S4(a) in the Supplementary Material], indicating that soil pixels affected the parameter estimation at the beginning of stem elongation. In addition, LAI and biomass estimated by model inversion also reached a significant correlation with biomass measured at flowering [$R^2 = 0.53$ and 0.61; see Fig. S4(b) and (c) in the Supplementary Material]. In general, the results indicate that the inverted parameters analyzed in this experiment increased their correlation with field measurements as GSs advanced, achieving the best results at the end of stem elongation and flowering.

C. Fertilizer Rate Detection

1) Ground-Level Sensors and Parameters Estimated by Model Inversion: Fertilizer rates were detected by GreenSeeker, Dualex, and the parameters estimated by model inversion (see Table III). As early as initial stem elongation (GS32), differences were detectable by GreenSeeker only. At the end of stem elongation (GS39), GreenSeeker and chlorophyll or anthocyanins, either measured with Dualex or estimated by model inversion, were able to distinguish between fertilized (N1 & N2) and unfertilized (N0) treatments. At flowering (GS65), GreenSeeker differentiated three N rates, whereas Chl, Flav, NBI from Dualex and inverted biomass, C_{ab}, and LAI distinguished between fertilized (N1 & N2) and unfertilized (N0) treatments. Finally, anthocyanins measured

This article has been accepted for inclusion in a future issue of this journal. Content is final as presented, with the exception of pagination.

TABLE III

WHEAT GREENSEEKER, DUALEX READINGS [CHLOROPHYLL (CHL-D), FLAVONOIDS (FLAV-D), ANTHOCYANINS (ANTH-D), AND N BALANCE INDEX (NBI-D)], AND PARAMETERS ESTIMATED BY MODEL INVERSION (BIOMASS, CHLOROPHYLL $a+b$ (C_{ab}), CAROTENOIDS (CAR), ANTHOCYANINS (ANTH), AND THE LAI) AT THREE DIFFERENT WHEAT GSS [INITIAL STEM ELONGATION (GS32), END OF STEM ELONGATION (GS39), AND FLOWERING (GS65)] FOR THE VARIOUS N RATE TREATMENTS (N0, N1, AND N2) APPLIED IN 2019

		Ground-level sensors				
N rate	**GS**	**GreenSeeker***	**Chl-D (μg cm^{-2})**	**Anth-D (d.u.)**	**Flav-D (d.u.)**	**NBI-D†**
N0	32	0.54 a‡	39.8	0.14	1.55	26
N1 & N2		0.58 b	40.8	0.13	1.51	27.4
N0	39	0.51 a	41.7 a	0.14 b	1.56	27.6
N1 & N2		0.59 b	43.8 b	0.13 a	1.55	28.6
N0	65	0.55 a	40.1 a	0.11	1.56 b	25.9 a
N1		0.63 b	44.6 b	0.10	1.52 a	29.5 b
N2		0.68 c	44.7 b	0.10	1.49 a	30.1 b
		Parameters estimated by model inversion				
		Biomass (kg ha^{-1})	**C_{ab} (μg cm^{-2})**	**Anth (μg cm^{-2})**	**Car (μg cm^{-2})**	**LAI (m^2 m^{-2})**
N0	32	-	41.8	4.47	10.1	2.58
N1 & N2		-	41.4	4.37	9.9	2.64
N0	39	3352	41.1 a	4.05 a	9.7	2.36
N1 & N2		3482	42.8 b	4.37 b	9.5	2.42
N0	65	3641 a	40.0 a	3.66	9.7	2.43 a
N1		3916 b	44.6 b	3.69	9.9	2.64 b
N2		4016 b	45.8 b	3.6	9.4	2.69 b

*Greenseeker readings are dimensionless measurements calculated as (R_{NIR}-R_{Red})/(R_{NIR}+R_{Red}), where R_{NIR} is the reflectance of active NIR light (774 nm) and R_{Red} is the reflectance of the active red light (656 nm).

†NBI-D is the ratio between Ch-D and Flav-D.

‡Within sensor, parameters and growth stage, values followed by different letters are significantly different according to Tukey's test at P ≤ 0.05. Abbreviations: d.u., dualex units.

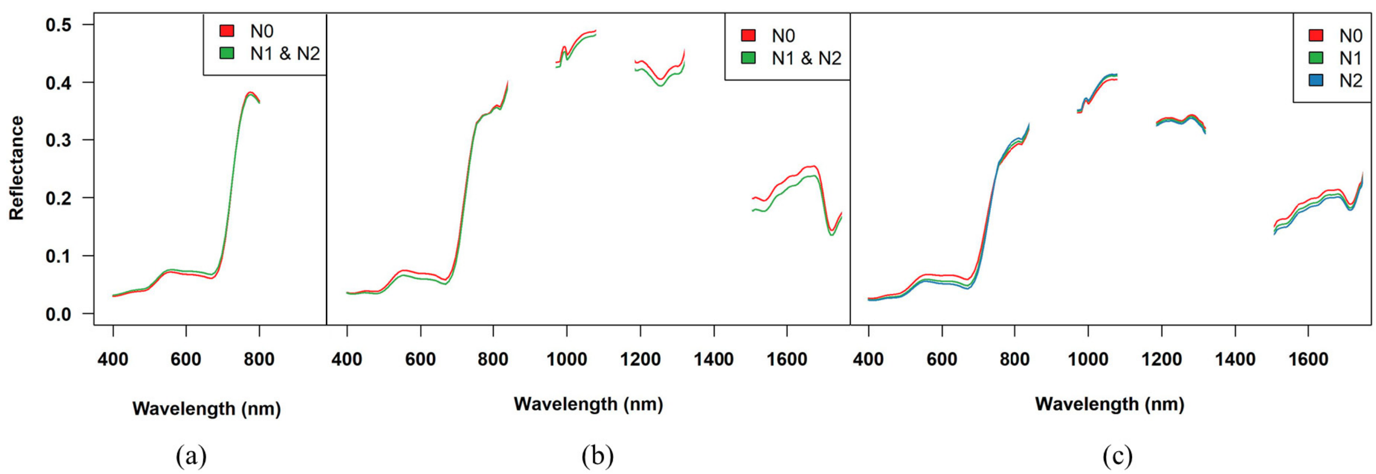

Fig. 5. Wheat average reflectance spectra from the various N rate treatments (N0, N1, and N2) obtained from images acquired by hyperspectral sensors [visible (400–740 nm), NIR (740–1000 nm), and SWIR (1000–1700 nm)] mounted on an aircraft at (a) initial stem elongation (GS32), (b) end of stem elongation (GS39), and (c) flowering (GS65) in 2019. Treatment N0 received 0 kg N ha^{-1} as fertilizer in 2019, N1 90 or 50 kg N ha^{-1}, and N2 130 or 90 kg N ha^{-1} in Control or fertilized plots in 2018.

with the Dualex device and the rest of the parameters (Anth and Car) estimated by model inversion did not separate fertilizer rates (see Table III).

2) Reflectance Spectra and Vegetation Indices: The different fertilizer rates applied in 2019 were also detected in the spectral data obtained from the aircraft (see Fig. 5). At the initial stem elongation (GS32), few differences were observed [see Fig. 5(a)]. Nevertheless, differences between reflectance spectra appeared at GS39, where the fertilized treatments (N1 & N2) presented lower reflectance in the visible region and SWIR than the unfertilized treatment (N0) [see Fig. 5(b)]. At GS65, the three N rate treatments were differentiated in the visible region, NIR and SWIR [see Fig. 5(c)].

In agreement with the spectra, at GS32, no differences in VIs were found between the N rate treatments, whereas, after GS39, differences between treatments appeared (see Table IV). At GS39, NDVI, blue/green/red indices, all chlorophyll (except MCARI), and all VNIR-SWIR (except $N_{1510,660}$) indices also differentiated between N0 and fertilized treatments (N1 & N2). At GS65, all structural, xanthophyll, BRI1,

TABLE IV

WHEAT VIs EXTRACTED FROM THE REFLECTANCE SPECTRA ACQUIRED BY AIRBORNE HYPERSPECTRAL SENSORS AT THREE DIFFERENT GSs [INITIAL STEM ELONGATION (GS32), END OF STEM ELONGATION (GS39), AND FLOWERING (GS65)] FOR THE VARIOUS N RATE TREATMENTS (N0, N1, AND N2) APPLIED IN 2019

		Vegetation indices					
		Structural		Xanthophyll		Blue/green/red	
N rate	GS	NDVI	OSAVI	PRI	PRIm4	BGI1	BRI1
N0	32	0.71	0.61	0.06	-0.27	0.42	0.39
N1 & N2		0.71	0.60	0.06	-0.27	0.43	0.40
N0	39	0.76 a	0.64	0.04	-0.25	0.52 a	0.52 a
N1 & N2		0.79 b	0.66	0.04	-0.25	0.56 b	0.55 b
N0		0.66 a	0.53 a	0.07 c	-0.27 a	0.40 a	0.35 a
N1	65	0.72 b	0.57 b	0.06 b	-0.26 b	0.42 b	0.39 b
N2		0.75 c	0.59 c	0.05 a	-0.25 c	0.42 b	0.41 c
		Chlorophyll-related indices					
		MCARI	TCARI/OSAVI	DCNI	NDRE	CCCI	SIF_{760}
N0	32	0.060	0.15	13.6	0.32	0.67	2.09
N1 & N2		0.058	0.15	13.9	0.32	0.69	2.10
N0	39	0.076	0.16 b	12.6 a	0.32 a	0.41 a	2.79 a
N1 & N2		0.074	0.15 a	13.3 b	0.34 b	0.50 b	2.86 b
N0		0.052 a	0.16 b	12.9 a	0.29 a	0.57 a	2.27 a
N1	65	0.052 a	0.14 a	14.1 b	0.33 b	0.72 b	2.44 b
N2		0.053 b	0.13 a	14.8 b	0.35 c	0.81 c	2.47 c
		SWIR- and VNIR-SWIR-based indices					
		NDNI	$OSAVI_{1510}$	$MCARI_{1510}$	$TCARI/OSAVI_{1510}$	$N_{1510,660}$	$N_{850,1150}$
N0	32	-	-	-	-	-	-
N1 & N2		-	-	-	-	-	-
N0	39	0.089 a	0.32 a	-0.050 a	-0.86 a	0.57	0.41 a
N1 & N2		0.096 b	0.34 b	-0.040 b	-0.75 b	0.57	0.44 b
N0		0.096 a	0.26 a	-0.040 a	-0.74 a	0.44 a	0.37 a
N1	65	0.099 b	0.29 b	-0.038 b	-0.70 b	0.50 b	0.40 b
N2		0.101 c	0.31 c	-0.037 c	-0.65 c	0.52 c	0.42 c

Within a column, values followed by different letters are significantly different according to Tukey's test at $P \leq 0.05$.

chlorophyll (NDRE, CCCI, and SIF_{760}), and all VNIR-SWIR indices distinguished the three fertilizer rates (see Table IV). Furthermore, in GS39 and GS65, the VNIR-SWIR indices that were modified to replace the 670-nm band with the 1510-nm band ($OSAVI_{1510}$, $MCARI_{1510}$, and $TCARI/OSAVI_{1510}$) were better N rate detectors than their corresponding VNIR indices, showing the potential of the SWIR.

D. Residual Effect Detection

1) Ground-Level Sensors and Parameters Estimated by Model Inversion: At the earliest stage of wheat (GS32), the residual effect was not detected, whereas, at the end of stem elongation (GS39) and flowering (GS65), the residual effect was similarly detected by the GreenSeeker and C_{ab} estimated by model inversion (see Table V). At both GSs, in the unfertilized wheat treatment (N0), the plots that received CAN+DMPSA in the previous season showed higher readings than the Control plots, with the readings of the plots fertilized with CAN or ASN + DMPP between these two readings. Moreover, at GS65, inverted biomass and the LAI detected the residual effect in all fertilized treatments in 2018. By contrast, the ability to detect the residual effect was low for Dualex readings (Chl, Anth, and the NBI showed differences between treatments at GS39 only) and the rest of the parameters estimated by model inversion (Anth and Car).

2) Reflectance Spectra and Vegetation Indices: Similar to ground-level sensors and inverted parameters, the residual effect was only detected in the spectra acquired from the unfertilized wheat treatments (see Fig. 6). At the initial stem elongation (GS32), differences between fertilized and Control treatments began to appear in the NIR [see Fig. 6(a)]. At GS39 and GS65, the three fertilized treatments presented lower reflectance in the visible region and SWIR and higher reflectance in the NIR than the Control [see Fig. 6(b) and (c)]. The CAN+DMPSA treatment, which showed the largest residual effect in the crop variables, GreenSeeker readings, and inverted C_{ab}, also presented the largest difference with the Control in the spectrum.

In addition, the structural (NDVI and OSAVI), blue/green (BGI1) and chlorophyll (NDRE and CCCI) indices, and SIF_{760} were able to detect the residual effect at the end of stem elongation (GS39), whereas, at flowering (GS65), it was detected by the structural (NDVI and OSAVI), chlorophyll (NDRE), and NIR-SWIR ($N_{850,1510}$) indices (see Table VI). The rest of the VIs calculated did not detect the residual effect (see Table S5 in the Supplementary Material). The values of the indices that detected the residual effect were higher in the CAN + DMPSA than in the Control plots, with the values of the plots previously fertilized with CAN or ASN + DMPP showing intermediate values. At the beginning of stem elongation (GS32), the residual effect was not detected (see Table S5 in the Supplementary Material). Therefore, SIF_{760} together with VIs that combine visible with blue, NIR, or red edge bands were the best residual effect detectors at the end of stem elongation, while the NIR-SWIR combination performed better at flowering.

TABLE V

WHEAT GREENSEEKER, DUALEX READINGS [CHLOROPHYLL (CHL-D), FLAVONOIDS (FLAV-D), ANTHOCYANINS (ANTH-D), AND N BALANCE INDEX (NBI-D)] AND PARAMETERS ESTIMATED BY MODEL INVERSION (BIOMASS, CHLOROPHYLL $a + b$ (C_{ab}), CAROTENOIDS (CAR), ANTHOCYANINS (ANTH), AND THE LAI) AT THREE DIFFERENT WHEAT GSS [INITIAL STEM ELONGATION (GS32), END OF STEM ELONGATION (GS39), AND FLOWERING (GS65)] IN THE UNFERTILIZED PLOTS (N0) IN 2019

		Ground-level sensors				
2018	GS	GreenSeeker*	Chl-D (μg cm^{-2})	Anth-D (d.u.)	Flav-D (d.u.)	NBI-D†
Control	32	0.50‡	37.1	0.15	1.59	23.6
CAN		0.55	41.3	0.14	1.55	26.7
ASN+DMPP		0.54	39.9	0.14	1.53	25.8
CAN+DMPSA		0.57	41.9	0.12	1.53	28.0
Control	39	0.46 a	38.1 a	0.16 b	1.62	23.8 a
CAN		0.51 ab	41.9 ab	0.14 ab	1.50	28.3 b
ASN+DMPP		0.54 ab	43.8 b	0.14 ab	1.53	29.0 b
CAN+DMPSA		0.57 b	43.3 b	0.13 a	1.58	27.9 ab
Control	65	0.50 a	37.8	0.11	1.63	24.0
CAN		0.57 ab	40.5	0.10	1.55	26.0
ASN+DMPP		0.57 ab	40.4	0.12	1.57	25.6
CAN+DMPSA		0.58 b	41.8	0.10	1.49	27.9
		Parameters estimated by model inversion				
		Biomass (kg ha^{-1})	C_{ab} (μg cm^{-2})	Anth (μg cm^{-2})	Car (μg cm^{-2})	LAI (m^2 m^{-2})
Control	32	-	41.2	4.45	10.33	2.60
CAN		-	43.2	4.28	9.22	2.68
ASN+DMPP		-	40.1	4.37	10.61	2.50
CAN+DMPSA		-	41.1	4.76	9.87	2.53
Control	39	3178	36.7 a	3.58	9.85	2.21
CAN		3418	41.5 ab	4.15	9.60	2.41
ASN+DMPP		3443	42.6 ab	4.17	10.04	2.35
CAN+DMPSA		3515	43.7 b	4.31	9.33	2.47
Control	65	3279 a	33.8 a	3.38	9.37	2.16 a
CAN		3786 b	41.2 ab	3.65	9.58	2.55 b
ASN+DMPP		3681 b	41.8 ab	3.84	10.00	2.47 b
CAN+DMPSA		3818 b	43.2 b	3.79	9.68	2.54 b

*Greenseeker readings are dimensionless measurements calculated as (R_{NIR}-R_{Red})/(R_{NIR}+R_{Red}), where R_{NIR} is the reflectance of active NIR light (774 nm) and R_{Red} is the reflectance of the active red light (656 nm).

†NBI-D is the ratio between Ch-D and Flav-D.

‡Within a column, values followed by different letters are significantly different according to Tukey's test at $P \leq 0.05$. Abbreviations: d.u., dualex units.

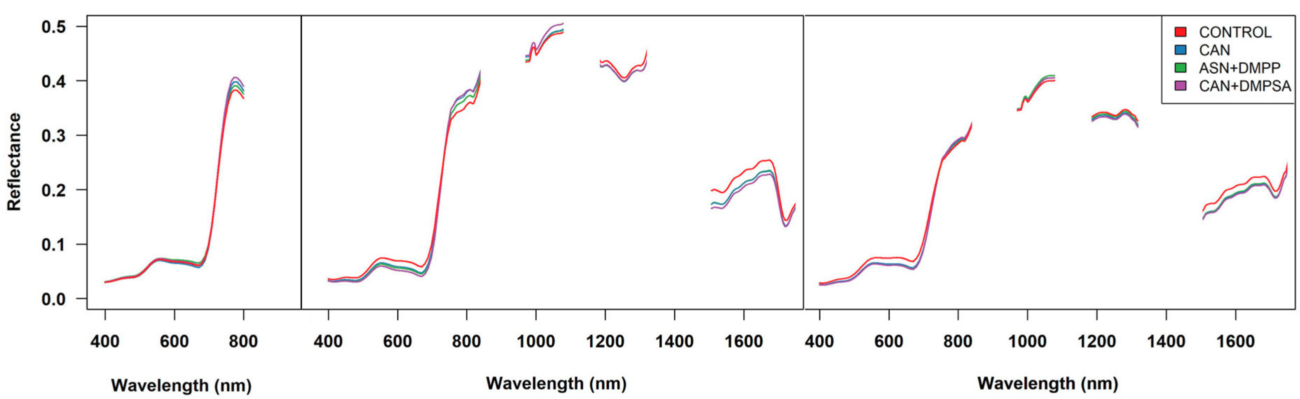

(a) (b) (c)

Fig. 6. Wheat average reflectance spectra from unfertilized N plots (N0) obtained from images acquired by hyperspectral sensors [visible (400–740 nm), NIR (740–1000 nm), and SWIR (1000–1700 nm)] mounted on an aircraft at (a) initial stem elongation (GS32), (b) the end of stem elongation (GS39), and (c) flowering (GS65) in 2019. Treatments in the legend were applied in the previous 2018 season and were 0 kg N ha^{-1} (Control) or 200 kg N ha^{-1} as CAN, as ASN blended with the nitrification inhibitor 3, 4-dimethylpyrazole phosphate (ASN + DMPP) or as CAN blended with the nitrification inhibitor 3, 4-dimethylpyrazole succinic (CAN + DMPSA).

E. Nitrogen Nutrition Index Detection by Ground-Level and Remote Sensors

Due to the good ability of the NNI in detecting N rates and the residual effect at flowering (see Fig. 3(a), and see Table S2 in the Supplementary Material), its correlation with ground-level sensors, inverted parameters, and VIs was evaluated as a proxy of detection (see Table VII). The highest correlations of the NNI with ground-level sensors were achieved

TABLE VI

WHEAT VIs EXTRACTED FROM THE REFLECTANCE SPECTRA ACQUIRED BY AIRBORNE HYPERSPECTRAL SENSORS AT TWO DIFFERENT GSs [END OF STEM ELONGATION (GS39) AND FLOWERING (GS65)] IN THE UNFERTILIZED PLOTS (N0) IN 2019

		Vegetation indices						
		Structural		Blue/green	Chlorophyll-related indices			VNIR-SWIR
2018	GS	NDVI	OSAVI	BGI1	NDRE	CCCI	SIF_{760}	$N_{850,1150}$
Control	39	0.69 a	0.59 a	0.49 a	0.27 a	0.19 a	2.50 a	0.38
CAN		0.78 ab	0.66 ab	0.51 ab	0.33 ab	0.43 ab	2.86 ab	0.43
ASN+DMPP		0.77 ab	0.65 ab	0.52 ab	0.32 ab	0.47 ab	2.86 ab	0.40
CAN+DMPSA		0.81 b	0.68 b	0.55 b	0.35 b	0.56 b	2.93 b	0.45
Control	65	0.62 a	0.49 a	0.39	0.26 a	0.49	2.20	0.34 a
CAN		0.67 ab	0.53 ab	0.40	0.30 ab	0.58	2.25	0.38 ab
ASN+DMPP		0.66 ab	0.54 ab	0.40	0.30 ab	0.59	2.28	0.38 ab
CAN+DMPSA		0.69 b	0.55 b	0.40	0.31 b	0.61	2.35	0.39 b

Within a column, values followed by the different letters are significantly different according to Tukey's test at P ≤ 0.05.

TABLE VII

COEFFICIENT OF DETERMINATION (R^2), RMSE, AND LEVEL OF SIGNIFICANCE (p-VALUE) FOR THE NNI AND GROUND-LEVEL SENSORS [GREENSEEKER, DUALEX READINGS (CHLOROPHYLL (CHL-D), FLAVONOIDS (FLAV-D), ANTHOCYANINS (ANTH-D), AND THE N BALANCE INDEX (NBI-D)], PARAMETERS ESTIMATED BY MODEL INVERSION (BIOMASS, CHLOROPHYLL $a + b$ (C_{ab}), CAROTENOIDS (CAR), ANTHOCYANINS (ANTH), AND THE LAI) AND DIFFERENT VIs EXTRACTED FROM THE REFLECTANCE SPECTRA ACQUIRED BY HYPERSPECTRAL SENSORS AT FLOWERING (GS65). ABBREVIATIONS: ns, NOT SIGNIFICANT

		R^2	RMSE	p-value
Ground-level sensors	GreenSeeker	0.75	0.052	<0.001
	Chl-D	0.65	0.062	<0.01
	Flav-D	0.54	0.070	<0.01
	Anth-D	0.26	0.089	ns
	NBI-D	0.68	0.059	<0.001
Parameters estimated by model inversion	Biomass	0.72	0.055	<0.001
	C_{ab}	0.72	0.059	<0.001
	Car	0.00	0.104	ns
	Anth	0.14	0.096	ns
	LAI	0.67	0.059	<0.01
Structural indices	NDVI	0.80	0.082	<0.001
	OSAVI	0.82	0.044	<0.001
Xanthophyll indices	PRI	0.73	0.044	<0.001
	PRIm4	0.80	0.047	<0.001
Blue/green/red ratio indices	BGI1	0.70	0.097	<0.001
	BRI1	0.76	0.051	<0.001
Chlorophyll-related indices	MCARI	0.55	0.070	<0.01
	TCARI/OSAVI	0.74	0.070	<0.001
	DCNI	0.69	0.058	<0.001
	NDRE	0.80	0.046	<0.001
	CCCI	0.82	0.044	<0.001
	SIF_{760}	0.88	0.049	<0.001
SWIR- and VNIR-SWIR-based indices	NDNI	0.68	0.050	<0.001
	$OSAVI_{1510}$	0.81	0.046	<0.001
	$MCARI_{1510}$	0.59	0.067	<0.01
	$TCARI/OSAVI_{1510}$	0.65	0.062	<0.01
	$N_{1510,660}$	0.78	0.048	<0.001
	$N_{850,1510}$	0.78	0.049	<0.001

by the GreenSeeker ($R^2 = 0.75$ and RMSE $= 0.052$) and the NBI from Dualex (see Table VII). Furthermore, the best performance among all pigments (either measured with Dualex or estimated by model inversion) was reached with chlorophyll. In this respect, C_{ab} estimated by model inversion obtained a greater correlation ($R^2 = 0.72$ and RMSE $= 0.059$) than the Chl measured with Dualex ($R^2 = 0.65$ and RMSE $= 0.062$), indicating that estimation of chlorophyll improves crop N status prediction. In addition, other inverted parameters, such as the LAI and biomass, also achieved a high correlation with the NNI. Finally, the rest of Dualex (Flav-D and Anth-D) and inverted pigments (Anth and Car) obtained the lowest correlations with the NNI (see Table VII).

Among the VIs, the best correlations with the NNI were obtained by chlorophyll-related indices, with the highest for SIF_{760} ($R^2 = 0.88$ and RMSE $= 0.049$) followed by CCCI and NDRE (see Table VII). The greenness or structural indices were also significantly correlated with NNI, and the PRIm4 xanthophyll index had a better correlation than the PRI. Finally, among the VNIR-SWIR indices, the $OSAVI_{1510}$ outperformed the others, achieving a similar correlation to its analog in the VNIR (OSAVI). Introducing the SWIR information slightly increased the correlation with NNI in the $MCARI_{1510}$ and slightly decreased in the $TCARI/OSAVI_{1510}$ (see Table VII).

Hence, these results emphasize that C_{ab} estimated by model inversion, SIF_{760}, the CCCI, and the indices that combine NIR-Red or NIR-Red Edge reflectance showed a better correlation than ground-level sensors in assessing crop N status, which reinforced their capability for N rates and residual effect detection.

IV. Discussion

The results of this study confirm the potential of ground and remote sensors for detecting wheat fertilized with different N rates and demonstrate, for the first time, the potential of these sensors for identifying the N residual effect in the crop. The ability of remote sensing to distinguish among N rates is relevant since it can provide information on the crop N status. However, most studies have traditionally been based on the application of spectral indices [21], while only a few studies have investigated the radiative transfer model inversions or solar-induced chlorophyll fluorescence [25], [27]. The earlier this detection occurs, the more suitable it would be for making recommendations prior to mid-season fertilization although, at early GSs, estimating the crop N status can be masked due to greater variations in biomass, the LAI, water availability conditions, or canopy structure [68]. Another limitation related to early fertilizer recommendation is crop water status and the presence of diseases and pests [2], which could be overcome by combining reflectance and thermal information in some cases [50], [71]. In this experiment, at the end of stem elongation, GreenSeeker readings, chlorophyll, and anthocyanin pigments (measured with Dualex and estimated by model inversion) are differentiated between unfertilized and fertilized treatment. Besides, in the reflectance spectra, distinctions between N rates were evident in the visible region and SWIR, caused by changes in photosynthetic activity, cell structure, and chemical bonds [73]. Higher N fertilization rates allow the plant to produce higher chlorophyll concentration and N-H bonds, increasing the light absorption in the visible region and SWIR. Therefore, most of the VIs differentiated between unfertilized and fertilized treatment, similar to other research that detected different N rates with hyperspectral [9] or proximal [74] sensors in wheat. Later at flowering, the reflectance spectra differentiated between N rates in the VNIR and SWIR, and consequently, most of the VIs and SIF_{760} also distinguished between the three N fertilizer rates, agreeing with other studies [75], [76]. At harvest, the effect of the fertilizer rates was observed on wheat grain N concentration and N output in the field samples analyzed. In relation to the yield, many authors observed an improvement with increasing N fertilizer application [74], [75] but, in our particular conditions, characterized by low rain during the end of winter and early spring, produced low tillering and limited the yield response to N. As a similar yield was recorded in all plots, differences between fertilizer rates appeared in grain N, which is usually harder to detect by remote sensing than in yield [77]. Besides, the crop data collected at flowering allowed the determination of the N uptake and the NNI calculation that reinforced the N fertilizer rate effect.

Beyond the benefits of nitrification inhibitors for reducing gaseous N losses, some authors explored the temporary soil N retention of these compounds [15], which may be an N source for the subsequent crops in the rotation [16]. Nitrification inhibitors may, therefore, be a valuable source of residual N, whose detection and quantification in crop rotations have not yet been solved, and to date, it has not been explored through remote sensing tools. In this study, the N residual effect was detected by spectral reflectance at the end of stem elongation and wheat flowering, showing the largest difference between the Control and CAN + DMPSA treatments. The reflectance was lower in the visible and SWIR, and higher in the NIR for CAN + DMPSA treatment, indicating a more healthy wheat crop. Therefore, several VIs and SIF_{760} showed the ability to detect the residual effect from DMPSA application in a maize/wheat rotation at the same GSs. The VIs that detected the residual effect in this experiment were the structural or greenness (NDVI and OSAVI), blue/green (BGI1) indices, chlorophyll (NDRE and CCCI), or NIR-SWIR ($N_{850,1510}$). Furthermore, the N residual effect was also detected by ground-level sensors and C_{ab}, biomass, and the LAI estimated by model inversion at the same GSs, coinciding with the results found by Quemada *et al.* [19] in a similar rotation. This suggests that inverted parameters, SIF_{760}, and VIs that include a red edge or at least one NIR band could be used to identify the N residual effect, making it possible to adjust fertilizer rates to actual crop requirements. This result is in agreement with previous studies that emphasize the advantage of using red edge narrow bands and NIR for estimating crop N status in wheat [77]. The crop data collected at flowering and harvest supported the residual effect detected with sensors.

In the same location, Alonso-Ayuso *et al.* [17] observed that ASN blended with the nitrification inhibitor DMPP had a higher residual effect than the conventional fertilizer in a maize/sunflower rotation. However, in this study, the residual effect coming from DMPP or conventional fertilizer was not observed in the following wheat crop. This apparent controversy may be due to the multiple factors that affect the N residual effect. On the one hand, high soil inorganic N content after crop harvest may lead to an N residual effect in the following crop. However, determining soil inorganic N may not be enough to account for this effect in the short term, as N retained in the crop litter and microbial biomass is slowly released over time [6], [19]. In addition, the residual effect may become evident when N fertilizer application is adjusted to crop requirements, whereas N overfertilization masks the residual effect [7].

Another novel result obtained in this experiment shows that SIF_{760} retrieval by the FLD method obtained a higher correlation with the NNI than the parameters estimated by model inversion and the VIs evaluated. This result agrees with recent studies that showed the ability of SIF_{760} to estimate crop physiological status [25] and differentiate between N treatments [44], [45]. This work confirmed the sensitivity of chlorophyll fluorescence to track changes in the photosynthetic capacity under different N treatments. Therefore, including chlorophyll fluorescence as an indicator of N deficiency enabled the tracking of the photosystem II photochemistry and the quantum yield of PSII electron transport reductions. This high correlation is probably due to the SIF_{760} emission originating exclusively from plants; therefore, its retrieval is not affected by the soil background. In addition, this study also demonstrates that the inverted C_{ab} had a greater correlation with crop N status than field measurements conducted with Dualex, reinforcing the potential of radiative transfer models and chlorophyll as the most reliable pigment for assessing N [23], [76].

Finally, some authors found significant relationships when comparing N concentration with NIR-SWIR-based indices in wheat [73], [25], trees and shrubs [24], and potato [23]. Nonetheless, in our study, the NIR-SWIR-based indices did not show an advantage over the structural and photosynthetic pigment indices based on the visible and NIR to detect N. The residual effect was only detected by $N_{850,1510}$ at flowering, suggesting that NIR-SWIR-based indices performed similar to the structural and photosynthetic pigment indices, while the VNIR-SWIR-based indices were unable to detect the residual effect. The main NIR-SWIR indices focused on the 1510-nm band, which is useful to pick up the absorption features corresponding to proteins (i.e., N-H bond stretches) [78]. However, in this subtle domain, the sharp absorption of water in the reflectance spectra introduces a bias that decreases the sensitivity for detecting N. Another possible explanation for not finding NIR-SWIR-based indices more sensitive than VNIR to crop N status is that wheat suffered from water stress during the growth cycle. Even if irrigation was uniformly delivered to compensate for water scarcity, SWIR bands are very sensitive to water presence and might have lost part of their capacity to identify crop nutritional status due to heterogeneous water availability. For all that, and considering the cost, the complexity of the operation, and the coarse resolution generally obtained by SWIR cameras [25], the contribution of SIF_{760} and VNIR indices is more convenient than VNIR-SWIR-extracted information. However, further investigation under rainfed conditions and with other crops remains necessary to define this information as accurately as possible.

V. Conclusion

Proximal and aerial sensors provided useful information for identifying wheat N fertilizer rates and residual effects. Optical ground-level sensors, plant traits estimated using biophysical modeling, solar-induced chlorophyll fluorescence (SIF_{760}), and VIs extracted by airborne hyperspectral sensors distinguished unfertilized and fertilized plots at wheat stem elongation and flowering, opening the opportunity to adjust N fertilization rates to crop demand. The residual effect of the conventional fertilizer blended with the DMPSA nitrification inhibitor applied on the previous maize in the rotation was detected by ground-level sensors, the estimated C_{ab} by model inversion, SIF_{760} and structural (NDVI and OSAVI), blue/green (BGI1), chlorophyll (NDRE and CCCI), and NIR-SWIR ($N_{850,1510}$) VIs calculated from the aircraft at the wheat stem elongation and flowering stages. Therefore, remote sensing has shown important potential as a tool to detect N fertilizer rates and the legacy of previous fertilizer applications in crop rotations. Further research will focus on understanding the differences in the residual effect of different fertilizers and fine-tune its detection using these technologies.

Acknowledgment

The authors would like to thank the staff from the La Chimenea Research Station (IMIDRA) for their essential technical support, J. López-Herrera and E. Pérez-Martín for georeferencing, and Javier López for his work in the laboratory.

References

[1] *Food and Agriculture Organization of the United Nations*, World Fertilizer Trends and Outlook to 2020. Rome, Italy, 2017.

[2] J. K. Ladha, H. Pathak, T. J. Krupnik, J. Six, and C. van Kessel, "Efficiency of fertilizer nitrogen in cereal production: Retrospects and prospects," *Adv. Agron.*, vol. 87, pp. 85–156, Oct. 2005, doi: 10.1016/S0065-2113(05)87003-8.

[3] B. Eickhout, A. F. Bouwman, and H. van Zeijts, "The role of nitrogen in world food production and environmental sustainability," *Agric. Ecosyst. Environ.*, vol. 116, nos. 1–2, pp. 4–14, Aug. 2006, doi: 10.1016/j.agee.2006.03.009.

[4] M. Quemada, M. Baranski, M. N. J. Nobel-de Lange, A. Vallejo, and J. M. Cooper, "Meta-analysis of strategies to control nitrate leaching in irrigated agricultural systems and their effects on crop yield," *Agric. Ecosyst. Environ.*, vol. 174, pp. 1–10, Jul. 2013, doi: 10.1016/j.agee.2013.04.018.

[5] C. Ravier, M. Quemada, and M.-H. Jeuffroy, "Use of a chlorophyll meter to assess nitrogen nutrition index during the growth cycle in winter wheat," *Field Crops Res.*, vol. 214, pp. 73–82, Dec. 2017, doi: 10.1016/j.fcr.2017.08.023.

[6] M. Sebilo, B. Mayer, B. Nicolardot, G. Pinay, and A. Mariotti, "Long-term fate of nitrate fertilizer in agricultural soils," *Proc. Nat. Acad. Sci. USA*, vol. 110, no. 45, pp. 18185–18189, Oct. 2013, doi: 10.1073/pnas.1305372110.

[7] M. Yan, G. Pan, J. M. Lavallee, and R. T. Conant, "Rethinking sources of nitrogen to cereal crops," *Glob. Chang. Biol.*, vol. 26, no. 1, pp. 191–199, Jan. 2020, doi: 10.1111/gcb.14908.

[8] J. N. Galloway *et al.*, "Transformation of the nitrogen cycle: Recent trends, questions, and potential solutions," *Science*, vol. 120, no. 5878, pp. 889–892, May 2008, doi: 10.1126/science.1136674.

[9] F. Li, B. Mistele, Y. Hu, X. Chen, and U. Schmidhalter, "Comparing hyperspectral index optimization algorithms to estimate aerial n uptake using multi-temporal winter wheat datasets from contrasting climatic and geographic zones in China and Germany," *Agricult. Forest Meteorol.*, vol. 180, pp. 44–57, Oct. 2013, doi: 10.1016/j.agrformet.2013.05.003.

[10] Y. Inoue *et al.*, "Simple and robust methods for remote sensing of canopy chlorophyll content: A comparative analysis of hyperspectral data for different types of vegetation," *Plant Cell Environ.*, vol. 39, no. 12, pp. 2609–2623, Sep. 2016, doi: 10.1111/pce.12815.

[11] D. Dourado-Neto *et al.*, "Multiseason recoveries of organic and inorganic nitrogen-15 in tropical cropping systems," *Soil Sci. Soc. Amer. J.*, vol. 74, no. 1, pp. 139–152, Jan. 2010, doi: 10.2136/sssaj2009.0192.

[12] X. Yan *et al.*, "Fertilizer nitrogen recovery efficiencies in crop production systems of China with and without consideration of the residual effect of nitrogen," *Environ. Res. Lett.*, vol. 9, no. 9, Sep. 2014, Art. no. 095002, doi: 10.1088/1748-9326/9/9/095002.

[13] *International Atomic Energy Agency*. Mangement of crop residues for sustainable crop production. Vienna, Austria, 2003.

[14] G. Pasda, R. Hähndel, and W. Zerulla, "Effect of fertilizers with the new nitrification inhibitor DMPP (3,4-dimethylpyrazole phosphate) on yield and quality of agricultural and horticultural crops," *Biol. Fertil. Soils*, vol. 34, no. 2, pp. 85–97, Aug. 2001, doi: 10.1007/s003740100381.

[15] Q. Ma *et al.*, "Responses of biotic and abiotic effects on conservation and supply of fertilizer N to inhibitors and glucose inputs," *Soil Biol. Biochem.*, vol. 89, pp. 72–81, Oct. 2015, doi: 10.1016/j.soilbio.2015.06.024.

[16] C. Liu, K. Wang, and X. Zheng, "Effects of nitrification inhibitors (DCD and DMPP) on nitrous oxide emission, crop yield and nitrogen uptake in a wheat–maize cropping system," *Biogeosciences*, vol. 10, no. 4, pp. 2427–2437, Apr. 2013, doi: 10.5194/bg-10-2427-2013.

[17] M. Alonso-Ayuso, J. L. Gabriel, and M. Quemada, "Nitrogen use efficiency and residual effect of fertilizers with nitrification inhibitors," *Eur. J. Agronomy*, vol. 80, pp. 1–8, Oct. 2016, doi: 10.1016/j.eja.2016.06.008.

[18] F. Wang *et al.*, "Nitrification inhibitor 3,4-dimethylpyrazole phosphate application during the later stage of apple fruit expansion regulates soil mineral nitrogen and tree carbon–nitrogen nutrition, and improves fruit quality," *Frontiers Plant Sci.*, vol. 11, pp. 1–15, Jun. 2020, doi: 10.3389/fpls.2020.00764.

[19] M. Quemada *et al.*, "Residual effect of synthetic nitrogen fertilizers and impact on soil nitrifiers," *Eur. J. Agronomy*, vol. 109, Sep. 2019, Art. no. 125917, doi: 10.1016/J.EJA.2019.125917.

[20] G. Lemaire, M. H. Jeuffroy, and F. Gastal, "Diagnosis tool for plant and crop N status in vegetative stage. Theory and practices for crop N management," *Eur. J. Agron.*, vol. 28, no. 4, pp. 614–624, May 2008, doi: 10.1016/j.eja.2008.01.005.

[21] C. S. T. Daughtry, C. L. Walthall, M. S. Kim, E. B. de Colstoun, and J. E. McMurtrey, "Estimating corn leaf chlorophyll concentration from leaf and canopy reflectance," *Remote Sens. Environ.*, vol. 74, no. 2, pp. 229–239, 2000, doi: 10.1016/S0034-4257(00)00113-9.

[22] P. J. Curran, "Remote sensing of foliar chemistry," *Remote Sens. Environ.*, vol. 30, no. 3, pp. 271–278, Dec. 1989, doi: 10.1016/0034-4257(89)90069-2.

[23] I. Herrmann, A. Karnieli, D. J. Bonfil, Y. Cohen, and V. Alchanatis, "SWIR-based spectral indices for assessing nitrogen content in potato fields," *Int. J. Remote Sens.*, vol. 31, no. 19, pp. 5127–5143, Oct. 2010, doi: 10.1080/01431160903283892.

[24] L. Serrano, J. Peñuelas, and S. L. Ustin, "Remote sensing of nitrogen and lignin in Mediterranean vegetation from AVIRIS data: Decomposing biochemical from structural signals," *Remote Sens. Environ.*, vol. 81, nos. 2–3, pp. 355–364, Aug. 2002, doi: 10.1016/S0034-4257(02)00011-1.

[25] C. Camino, V. González-Dugo, P. Hernández, J. C. Sillero, and P. J. Zarco-Tejada, "Improved nitrogen retrievals with airborne-derived fluorescence and plant traits quantified from VNIR-SWIR hyperspectral imagery in the context of precision agriculture," *Int. J. Appl. Earth Observ. Geoinf.*, vol. 70, pp. 105–117, Aug. 2018, doi: 10.1016/j.jag.2018.04.013.

[26] S. Jacquemoud *et al.*, "PROSPECT + SAIL models: A review of use for vegetation characterization," *Remote Sens. Environ.*, vol. 113, pp. S56–S66, Sep. 2009, doi: 10.1016/j.rse.2008.01.026.

[27] Z. Li *et al.*, "Remote sensing of leaf and canopy nitrogen status in winter wheat (Triticum aestivum L.) based on N-PROSAIL model," *Remote Sens.*, vol. 10, no. 9, pp. 1–18, Sep. 2018, doi: 10.3390/rs10091463.

[28] P. J. Zarco-Tejada *et al.*, "Assessing vineyard condition with hyperspectral indices: Leaf and canopy reflectance simulation in a row-structured discontinuous canopy," *Remote Sens. Environ.*, vol. 99, no. 3, pp. 271–287, Nov. 2005, doi: 10.1016/J.RSE.2005.09.002.

[29] Z. Wang, A. K. Skidmore, R. Darvishzadeh, U. Heiden, M. Heurich, and T. Wang, "Leaf nitrogen content indirectly estimated by leaf traits derived from the PROSPECT model," *IEEE J. Sel. Topics Appl. Earth Observ. Remote Sens.*, vol. 8, no. 6, pp. 3172–3182, Jun. 2015, doi: 10.1109/JSTARS.2015.2422734.

[30] J. B. Féret, K. Berger, F. de Boissieu, and Z. Malenovský, "PROSPECT-PRO for estimating content of nitrogen-containing leaf proteins and other carbon-based constituents," *Remote Sens. Environ.*, vol. 252, Jan. 2021, Art. no. 112173, doi: 10.1016/j.rse.2020.112173.

[31] E. J. Botha, B. Leblon, B. J. Zebarth, and J. Watmough, "Non-destructive estimation of wheat leaf chlorophyll content from hyperspectral measurements through analytical model inversion," *Int. J. Remote Sens.*, vol. 31, no. 7, pp. 1679–1697, Apr. 2010, doi: 10.1080/01431160902926574.

[32] M. Meroni *et al.*, "Remote sensing of solar-induced chlorophyll fluorescence: Review of methods and applications," *Remote Sens. Environ.*, vol. 113, no. 10, pp. 2037–2051, Oct. 2009, doi: 10.1016/j.rse.2009.05.003.

[33] B. Genty, J. M. Briantais, and N. R. Baker, "The relationship between the quantum yield of photosynthetic electron transport and quenching of chlorophyll fluorescence," *Biochimica et Biophys. Acta (BBA)-Gen. Subjects*, vol. 990, no. 1, pp. 87–92, Jan. 1989, doi: 10.1016/S0304-.4165(89)80016-9.

[34] C. Lu and J. Zhang, "Photosynthetic CO^2 assimilation, chlorophyll fluorescence and photoinhibition as affected by nitrogen deficiency in maize plants," *Plant Sci.*, vol. 151, no. 2, pp. 135–143, Feb. 2000, doi: 10.1016/S0168-9452(99)00207-1.

[35] X. Jin, G. Yang, C. Tan, and C. Zhao, "Effects of nitrogen stress on the photosynthetic CO_2 assimilation, chlorophyll fluorescence and sugar-nitrogen ratio in corn," *Sci. Rep.*, vol. 5, no. 1, p. 9311, Apr. 2015, doi: 10.1038/srep09311.

[36] C. Camino, V. Gonzalez-Dugo, P. Hernandez, and P. J. Zarco-Tejada, "Radiative transfer Vcmax estimation from hyperspectral photosynthetic performance in rainfed and irrigated plant phenotyping trials," *Remote Sens. Environ.*, vol. 231, Sep. 2019, Art. no. 111186, doi: 10.1016/j.rse.2019.05.005.

[37] H. R. Bolhar-Nordenkampf, S. P. Long, N. R. Baker, G. Oquist, U. Schreiber, and E. G. Lechner, "Chlorophyll fluorescence as a probe of the photosynthetic competence of leaves in the field: A review of current instrumentation," *Funct. Ecol.*, vol. 3, no. 4, pp. 497–514, 1989, doi: 10.2307/2389624.

[38] Z. Kolber, D. Klimov, G. Ananyev, U. Rascher, J. Berry, and B. Osmond, "Measuring photosynthetic parameters at a distance: Laser induced fluorescence transient (LIFT) method for remote measurements of photosynthesis in terrestrial vegetation," *Photosynthesis Res.*, vol. 84, nos. 1–3, pp. 121–129, Jun. 2005, doi: 10.1007/s11120-005-5092-1.

[39] J. A. Plascyk and F. C. Gabriel, "The Fraunhofer line discriminator MKII—An airborne instrument for precise and standardized ecological luminescence measurement," *IEEE Trans. Instrum. Meas.*, vol. IM-24, no. 4, pp. 306–313, Dec. 1975, doi: 10.1109/TIM.1975.4314448.

[40] R. Calderón, J. Navas-Cortés, and P. Zarco-Tejada, "Early detection and quantification of verticillium wilt in olive using hyperspectral and thermal imagery over large areas," *Remote Sens.*, vol. 7, no. 5, pp. 5584–5610, May 2015, doi: 10.3390/rs70505584.

[41] P. J. Zarco-Tejada *et al.*, "Previsual symptoms of Xylella fastidiosa infection revealed in spectral plant-trait alterations," *Nature Plants*, vol. 4, no. 7, pp. 432–439, Jun. 2018, doi: 10.1038/s41477-018-0189-7.

[42] G. H. Mohammed *et al.*, "Remote sensing of solar-induced chlorophyll fluorescence (SIF) in vegetation: 50 years of progress," *Remote Sens. Environ.*, vol. 231, Sep. 2019, Art. no. 111177, doi: 10.1016/j.rse.2019.04.030.

[43] P. J. Zarco-Tejada, V. González-Dugo, and J. A. J. Berni, "Fluorescence, temperature and narrow-band indices acquired from a UAV platform for water stress detection using a micro-hyperspectral imager and a thermal camera," *Remote Sens. Environ.*, vol. 117, pp. 322–337, Feb. 2012, doi: 10.1016/J.RSE.2011.10.007.

[44] M. Quemada, J. L. Gabriel, and P. Zarco-Tejada, "Airborne hyperspectral images and ground-level optical sensors as assessment tools for maize nitrogen fertilization," *Remote Sens.*, vol. 6, no. 4, pp. 2940–2962, Mar. 2014, doi: 10.3390/rs6042940.

[45] M. P. Cendrero-Mateo *et al.*, "Plant chlorophyll fluorescence: Active and passive measurements at canopy and leaf scales with different nitrogen treatments," *J. Experim. Botany*, vol. 67, no. 1, pp. 275–286, Jan. 2016, doi: 10.1093/jxb/erv456.

[46] P. J. Zarco-Tejada, M. V. González-Dugo, and E. Fereres, "Seasonal stability of chlorophyll fluorescence quantified from airborne hyperspectral imagery as an indicator of net photosynthesis in the context of precision agriculture," *Remote Sens. Environ.*, vol. 179, pp. 89–103, Jun. 2016, doi: 10.1016/j.rse.2016.03.024.

[47] D. J. Greenwood, G. Lemaire, G. Gosse, P. Cruz, A. Draycott, and J. J. Neeteson, "Decline in percentage N of C3 and C4 crops with increasing plant mass," *Ann. Botany*, vol. 66, no. 4, pp. 425–436, Oct. 1990, doi: 10.1093/oxfordjournals.aob.a088044.

[48] E. Justes *et al.*, "Determination of a critical nitrogen dilution curve for winter wheat crops," *Ann. Botany*, vol. 74, no. 4, pp. 397–407, Oct. 1994, doi: 10.1006/anbo.1994.1133.

[49] N. Ziadi *et al.*, "Determination of a critical nitrogen dilution curve for spring wheat," *Agronomy J.*, vol. 102, no. 1, pp. 241–250, Jan. 2010, doi: 10.2134/agronj2009.0266.

[50] J. L. Pancorbo *et al.*, "Simultaneous assessment of nitrogen and water status in winter wheat using hyperspectral and thermal sensors," *Eur. J. Agron.*, vol. 127, Jul. 2021, Art. no. 126287, doi: 10.1016/j.eja.2021.126287.

[51] *World Reference Base for Soil Resources. International Soil Classification System for Naming Soils and Creating Legends for Soil Maps*. World Soil Resources Reports, FAO, Rome, Italy, 2014, no. 106.

[52] J. L. Gabriel, R. Muñoz-Carpena, and M. Quemada, "The role of cover crops in irrigated systems: Water balance, nitrate leaching and soil mineral nitrogen accumulation," *Agricult., Ecosyst. Environ.*, vol. 155, pp. 50–61, Jul. 2012, doi: 10.1016/j.agee.2012.03.021.

[53] U. Meier, "Phenological growth stages and BBCH-identification keys of weed species," in *Growth of Stages Mono- and Dicotyledonous Plants*, U. Meier, ed. Berlin, Germany: Blackwell Wissenschafts-Verlag, 1997, pp. 135–139.

[54] D. R. Keeney and D. W. Nelson, "Nitrogen—Inorganic forms," in *Methods of Soil Analysis, Part 2, Chemical and Micribiological Properties*, A. L. Page, ed. Madison, WI, USA: American Sociey of Agronomy, 1982, pp. 643–693.

[55] W. M. Crooke and W. E. Simpson, "Determination of ammonium in Kjeldahl digests of crops by an automated procedure," *J. Sci. Food Agricult.*, vol. 22, no. 1, pp. 9–10, Jan. 1971, doi: 10.1002/jsfa.2740220104.

[56] N. Tremblay, Z. Wang, and Z. G. Cerovic, "Sensing crop nitrogen status with fluorescence indicators. A review," *Agronomy for Sustain. Develop.*, vol. 32, no. 2, pp. 451–464, Jul. 2011, doi: 10.1007/s13593-011-0041-1.

[57] C. Gueymard, "SMARTS, A simple model of the atmospheric radiative transfer of sunshine: Algorithms and performance assessment," Florida Sol. Energy Center, Cocoa, FL, USA, Tech. Rep., FSEC-PF-270-95, 1995.

[58] C. Gueymard, "Parameterized transmittance model for direct beam and circumsolar spectral irradiance," *Sol. Energy.*, vol. 71, no. 5, pp. 325–346, Nov. 2001, doi: 10.1016/S0038-092X(01)00054-8.

[59] G. M. Smith and E. J. Milton, "The use of the empirical line method to calibrate remotely sensed data to reflectance," *Int. J. Remote Sens.*, vol. 20, no. 13, pp. 2653–2662, 1999, doi: 10.1080/014311699211994.

[60] W. Verhoef and H. Bach, "Coupled soil-leaf-canopy and atmosphere radiative transfer modeling to simulate hyperspectral multi-angular surface reflectance and TOA radiance data," *Remote Sens. Environ.*, vol. 109, no. 2, pp. 166–182, Jul. 2007, doi: 10.1016/j.rse.2006.12.013.

[61] G. H. Suits, "The calculation of the directional reflectance of a vegetative canopy," *Remote Sens. Environ.*, vol. 2, no. 2, pp. 117–125, 1972, doi: 10.1016/0034-4257(71)90085-X.

[62] M. Weiss, F. Baret, R. B. Myneni, A. Pragnère, and Y. Knyazikhin, "Investigation of a model inversion technique to estimate canopy biophysical variables from spectral and directional reflectance data," *Agronomie*, vol. 20, no. 1, pp. 3–22, Jan. 2000, doi: 10.1051/agro:2000105.

[63] A. Damm *et al.*, "Modeling the impact of spectral sensor configurations on the FLD retrieval accuracy of sun-induced chlorophyll fluorescence," *Remote Sens. Environ.*, vol. 115, no. 8, pp. 1882–1892, Aug. 2011, doi: 10.1016/j.rse.2011.03.011.

[64] J. W. Rouse, R. H. Haas, J. A. Schell, D. W. Deering, and J. Harlan, "Monitoring the vernal advancement of retrogradation (green wave effect) of natural vegetation," NASA/GSFC, Greenbelt, MD, USA, Tech. Rep. E75-10354, 1974, pp. 1–371.

[65] G. Rondeaux, M. Steven, and F. Baret, "Optimization of soil-adjusted vegetation indices," *Remote Sens. Environ.*, vol. 55, no. 2, pp. 95–107, Feb. 1996, doi: 10.1016/0034-4257(95)00186-7.

[66] J. A. Gamon, J. Peñuelas, and C. B. Field, "A narrow-waveband spectral index that tracks diurnal changes in photosynthetic efficiency," *Remote Sens. Environ.*, vol. 41, no. 1, pp. 35–44, 1992, doi: 10.1016/0034-4257(92)90059-S.

[67] R. Hernández-Clemente, R. M. Navarro-Cerrillo, L. Suárez, F. Morales, and P. J. Zarco-Tejada, "Assessing structural effects on PRI for stress detection in conifer forests," *Remote Sens. Environ.*, vol. 115, no. 9, pp. 2360–2375, Sep. 2011, doi: 10.1016/j.rse.2011.04.036.

[68] D. Haboudane, J. R. Miller, N. Tremblay, P. J. Zarco-Tejada, and L. Dextraze, "Integrated narrow-band vegetation indices for prediction of crop chlorophyll content for application to precision agriculture," *Remote Sens. Environ.*, vol. 81, nos. 2–3, pp. 416–426, Aug. 2002, doi: 10.1016/S0034-4257(02)00018-4.

[69] P. Chen, D. Haboudane, N. Tremblay, J. Wang, P. Vigneault, and B. Li, "New spectral indicator assessing the efficiency of crop nitrogen treatment in corn and wheat," *Remote Sens. Environ.*, vol. 114, no. 9, pp. 1987–1997, Sep. 2010, doi: 10.1016/j.rse.2010.04.006.

[70] E. M. Barnes, T. R. Clarke, S. E. Richards, P. D. Colaizzi, J. Haberland, and M. Kostrzewski, "Coincident detection of crop water stress, nitrogen status and canopy density using ground-based multispectral data," *Proc. 5th Int. Conf. Precis. Agricult.*, Bloomington, MN, USA, 2000, pp. 1–15.

[71] G. J. Fitzgerald, D. Rodriguez, L. K. Christensen, R. Belford, V. O. Sadras, and T. R. Clarke, "Spectral and thermal sensing for nitrogen and water status in rainfed and irrigated wheat environments," *Precis. Agricult.*, vol. 7, no. 4, pp. 233–248, Jul. 2006, doi: 10.1007/s11119-006-9011-z.

[72] R Core Team. (2019). *R: A Language and Environment for Statistical Computing*. R Foundation for Statistical Computing, Vienna, Austria. [Online]. Available: https://www.R-project.org/

[73] G. R. Mahajan, R. N. Sahoo, R. N. Pandey, V. K. Gupta, and D. Kumar, "Using hyperspectral remote sensing techniques to monitor nitrogen, phosphorus, sulphur and potassium in wheat (Triticum aestivum L.)," *Precis. Agricult.*, vol. 15, no. 5, pp. 499–522, Feb. 2014, doi: 10.1007/s11119-014-9348-7.

[74] W. R. Raun *et al.*, "Optical sensor-based algorithm for crop nitrogen fertilization," *Commun. Soil Sci. Plant Anal.*, vol. 36, nos. 19–20, pp. 2759–2781, 2005, doi: 10.1080/00103620500303988.

[75] L. M. Arregui, B. Lasa, A. Lafarga, I. Irañeta, E. Baroja, and M. Quemada, "Evaluation of chlorophyll meters as tools for n fertilization in winter wheat under humid Mediterranean conditions," *Eur. J. Agronomy*, vol. 24, no. 2, pp. 140–148, Feb. 2006, doi: 10.1016/j.eja.2005.05.005.

[76] N. Tremblay, Z. Wang, and C. Belec, "Performance of dualex in spring wheat for crop nitrogen status assessment, yield prediction and estimation of soil nitrate content," *J. Plant Nutrition*, vol. 33, no. 1, pp. 57–70, 2010, doi: 10.1080/01904160903391081.

[77] L. Prey and U. Schmidhalter, "Simulation of satellite reflectance data using high-frequency ground based hyperspectral canopy measurements for in-season estimation of grain yield and grain nitrogen status in winter wheat," *ISPRS J. Photogramm. Remote Sens.*, vol. 149, pp. 176–187, Mar. 2019, doi: 10.1016/j.isprsjprs.2019.01.023.

[78] R. F. Kokaly and R. N. Clark, "Spectroscopic determination of leaf biochemistry using band-depth analysis of absorption features and stepwise multiple linear regression," *Remote Sens. Environ.*, vol. 67, no. 3, pp. 267–287, Mar. 1999, doi: 10.1016/S0034-4257(98)00084-4.

María D. Raya-Sereno was born in Córdoba, Spain, in 1991. She received the degree in environmental science from the University of Córdoba, Córdoba, in 2014, and the M.S. degree in planning and management of territorial and local development from the University of Seville, Seville, Spain, in 2015. She is pursuing the Ph.D. degree in environmental technology for sustainable agriculture with the Universidad Politécnica de Madrid, Madrid, Spain.

From 2016 to 2018, she was a Research Assistant with the Institute of Natural Resources and Agrobiology, National Research Council (CSIC), Seville. Her recent research focuses on agricultural remote sensing, water and nitrogen management, crop growth monitoring, adaptations to climate change, and data assimilation.

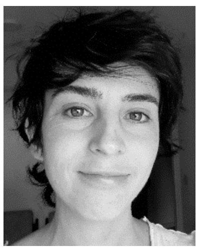

María Alonso-Ayuso received the M.S. degree in agronomic engineering and the Ph.D. degree in agronomy from the Universidad Politécnica de Madrid, Madrid, Spain, in 2011 and 2018, respectively.

From 2018 to 2020, she was a Post-Doctoral Researcher with the Department of Agricultural Production, Universidad Politécnica de Madrid. Since May 2021, she has been a Post-Doctoral Research Fellow with the Soil Management and Global Change Group, Spanish National Research Council (CSIC), Zaragoza, Spain. She is the author of 18 articles. Her research interests include cropping system diversification, soil-crop modeling, or N fertilization. She is particularly interested in the assessment of techniques that increase the sustainability of agroecosystems.

Dr. Alonso-Ayuso was a recipient of the Spanish Weed Science Society Award for her Ph.D. in 2019.

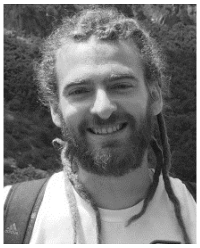

José L. Pancorbo was born in Barcelona, Spain, in 1990. He received the M.S. degree in forest engineering from the Universidad Politécnica de Madrid, Madrid, Spain, in 2017, where he is pursuing the Ph.D. degree in environmental technology for sustainable agriculture.

He is a member of the Research Centre for the Management of Agricultural and Environmental Risks (CEIGRAM), Universidad Politécnica de Madrid, and has participated in different international congress and research projects related to environmental protection. He has different publications in the field of precision agriculture and sensor evaluation. He is working in multisensors' approaches for estimating plant biophysical parameters. His research interests include remote sensing and its application in vegetation monitoring.

José L. Gabriel received the Ph.D. degree in agronomy from the Universidad Politécnica de Madrid, Madrid, Spain, in 2011.

He has a permanent position as the Main Researcher at the National Institute for Agricultural and Food Research and Technology (INIA), Madrid, since 2017. He has 12 years of experience at the Universidad Politécnica de Madrid, the University of Florida, Gainesville, FL, USA, 2010, and the Université catholique de Louvain, Ottignies-Louvain-la-Neuve, Belgium, from 2012 to 2013. He has participated in five national projects (one of them as IP), six European (three of them as IP), two regional, and several internal projects and contracts with private companies. He is the author of 30 SCI publications (most of them in the Q1) and the editor of one book, more than 20 book chapters, 30 international communications, ten nationals, and some divulgation articles in stakeholder magazines. His research lines have dealt with sustainable agricultural systems, focusing on water and nitrogen use efficiency and cover crops use in order to increase crop yield but reducing contamination problems, based on the use of field experiments proximal/remote sensors and simulation models.

Dr. Gabriel has been prized by the Fertiberia Company and the Universidad Politécnica de Madrid for his Ph.D. and by the Spanish Society for Horticultural Sciences (SECH) for his trajectory.

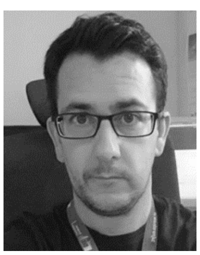

Carlos Camino was born in Palencia, Spain, in 1977. He received the M.S.C. degree in biology from the University of Jaén, Jaén, Spain, in 2003, and the Ph.D. degree in biology from the University of Córdoba, Córdoba, Spain, in 2019.

From 2010 to 2015, he was a Research Assistant with the State Meteorological Agency, Córdoba. After that, he has developed his research career at the Institute for Sustainable Agriculture, Córdoba, from 2015 to 2019. Since 2019, he has continued his research in the use of high-resolution hyperspectral and thermal imagery in the Joint Research Centre, Ispra, Italy, which belongs to the European Commission. He is the author of more than 15 articles. His research interests include high-resolution hyperspectral and thermal imagery, early detection of plant pests, quantification of nitrogen at canopy scales, radiative transfer modeling, and machine learning applied to estimate plant traits.

Pablo J. Zarco-Tejada received the degree in agricultural engineering from the University of Córdoba, Córdoba, Spain, in 1995, the M.Sc. degree in remote sensing from the University of Dundee, Dundee, U.K., in 1997, and the Ph.D. degree in earth and space science from York University, Toronto, ON, Canada, in 2000.

He has been a Faculty Member for remote sensing with the University of California at Davis, Davis, CA, USA, the Director of the Institute for Sustainable Agriculture (IAS), National Research Council (CSIC), Córdoba, and a Senior Scientist with the European Commission, Joint Research Centre (JCR), Ispra, Italy. He is a Professor of remote sensing and precision agriculture with the Faculty of Veterinary and Agricultural Sciences of Engineering, The University of Melbourne, Melbourne, VIC, Australia, and an Honorary Scientist with IAS-CSIC. As the Leader of the HyperSens Laboratory, Córdoba, he focuses on remote sensing for biotic and abiotic stress detection using hyperspectral and thermal images acquired by manned and unmanned aircraft systems. A highly cited research in 2019 and 2020, he is the author of more than 150 articles published in international journals.

Dr. Zarco-Tejada received awards in Spain, the U.K., and Canada. He is also an Associate Editor of *Remote Sensing of Environment* and *European Journal of Agronomy*.

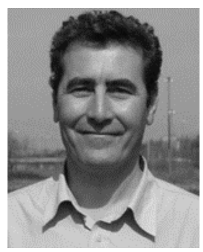

Miguel Quemada received the degree in agricultural engineering from the Universidad Politécnica de Madrid (UPM), Madrid, Spain, and the Ph.D. degree in agronomy from the University of Georgia, Athens, GA, USA, in 1995.

He was a Faculty Member with the Universidad Pública de Navarra, Pamplona, Spain, for five years, first as a Researcher and then as an Associate Professor. Since 2000, he moved to UPM, where he became a Professor in 2008. He is a Senior Scientist with the Research Centre for the Management of Agricultural and Environmental Risks (CEIGRAM), Universidad Politécnica de Madrid, Madrid, Spain. He also collaborates with the Hydrology and Remote Sensing Laboratory, Beltsville, MD, USA, The University of Newcastle, Callaghan, U.K., the Universidad de Santiago, Santiago, Chile, and the International Maize and Wheat Improvement Center (CIMMYT), Texcoco, Mexico. His field of expertise is nitrogen (N) and water management in agricultural systems, researching strategies that increase crop N use efficiency and minimize the environmental impact of N emissions. He is particularly interested in combining research at a field scale with new monitoring technologies to enhance the sustainability of cropping systems. He is the author of more than 70 scientific articles published in SCI international journals; some of them are highly cited.

Dr. Quemada is also a member of the European Expert Nitrogen Panel and acts as an External Expert for the European Commission on assessing research, technology, and development (RTD) projects. He is also an Associate Editor of *Agronomy for Sustainable Development* and *European Journal of Agronomy*.